Murphy et al. 2005; Nørgaard et al. 2005) because it enables the detection of crystals, and in particular, differences between crystal forms. Therefore, Microscopic Laser Raman Spectroscopy/Mapping (MLRSM) was employed in the present study to microscopically and chemically detect TBR crystals in transdermal tapes. The applicability of this spectroscopic analytical method was examined both for the purpose of quality control (i.e., to confirm the crystals of TBR in the matrix), as well as with the aim of enhancing our understanding of relevant quality attributes of prototype pharmaceuticals in various stages of development.

2. Investigations and results

2.1. Determination of a unique wave number range in the Raman spectrum for TBR in model tapes

A typical Raman spectrum obtained from the TBR reference standard substance is shown in Fig. 1. Typical spectra of placebo tape (a) and model tape (b) of rubber matrices are shown in Figs. 2 and 3, respectively. To find characteristic wave numbers of TBR, these spectra were compared with the Raman spectrum obtained from a model tape. The peak bending vibration of C–C at 415cm^{-1} was used as the characteristic peak of TBR, and the integrated values obtained from the wave number range from 420 cm^{-1} to 400 cm^{-1} were used for making the Raman chemical maps.

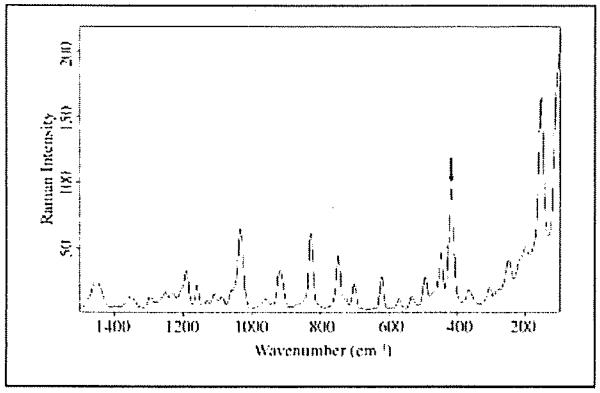

Fig. 1: Typical Raman spectrum of the TBR reference standard. The peak at 415 cm^{-1} was chosen as characteristic, because no interfering peak was observed in the vicinity of this peak

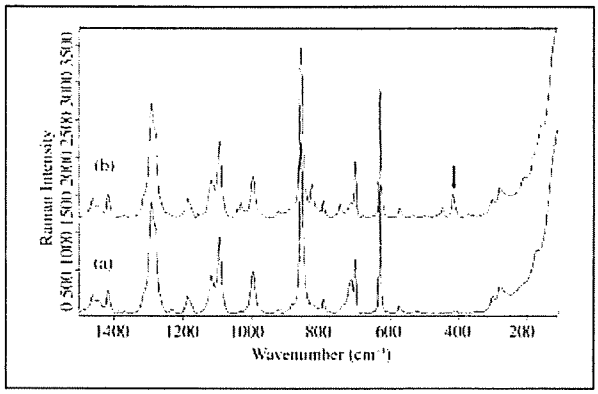

Fig. 2: Typical Raman spectra of placebo (a, rubber matrix) and model tape (b, rubber matrix). The arrow indicates the peak chosen for the specific detection of TBR. Comparatively strong intensity was observed

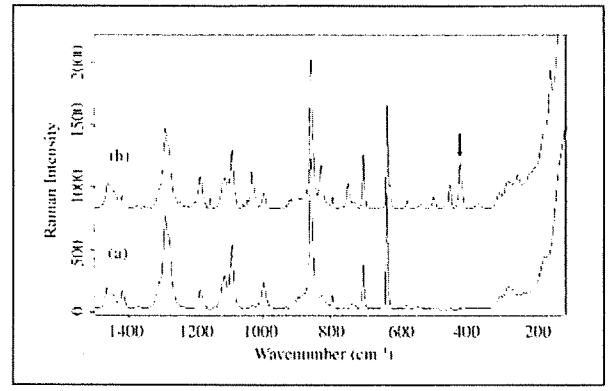

Fig. 3: Typical Raman spectra of placebo (a, acrylic matrix) and model tape (b, acrylic matrix). The very similar Raman spectrum of placebo tape was observed compared with that of the rubber matrix, because the absorption of supporting boards that were made from PET was also detected

2.2. Optical micrograph and Raman chemical mapping of the crystals of TBR in a rubber matrix

Figure 4a shows the micrograph of a 600 × 500 µm area in the R-10 sample. An enlarged micrograph (200 × 200 µm) is shown in Fig. 4b. Pillar-shaped crystals (short, 1 µm–2 µm; long, 10 µm–20 µm) that formed in lumps were observed. Figure 4c and d show the three-dimensional (3D) map and the Raman chemical map that corresponds with the area in Fig. 4b. In the Raman chemical map, the distribution of TBR in the matrix corresponded with the distribution of crystals in the optical micrograph. The Raman absorbance intensity corresponded with the distribution of optically observed TBR.

2.3. Optical micrograph and Raman chemical mapping of the crystals of TBR in an acrylic matrix

A micrograph of a 600 × 500 µm area and an enlarged micrograph of a 200 × 200 µm area of the A-20 sample are shown in Fig. 5a and b, respectively. In Figure 5c and d, the respective 3D chemical map and Raman chemical map are given that correspond to Fig. 5b. A lump of crystals with radiating branches was observed in the matrix. The Raman chemical map of TBR corresponding to the micrograph was obtained. The Raman chemical maps, which show the distribution of Raman chemical intensity, indicated trace amounts of crystal growth.

2.4. Shapes of crystals of TBR in two types of matrix

The micrograph of early-stage TBR crystallization in an acrylic matrix is shown in Fig. 6a. A lump of crystals with radiating branches was observed. Figure 6b shows the micrograph obtained approximately at the level of the top of branch of the crystal. The findings suggest that the pillar-shaped crystals were successively generated at the top of branches, and that the branches grew radially from the core. In case of the rubber matrix, pillar-shaped crystals that formed individual lumps were observed, as shown in Fig. 4a and b. No signs of a core were observed, and lumps of pillar-shaped crystals occurred individually in the matrix. These findings suggest that the TBR crystal growth mechanism differs in the two types of matrix analyzed here. Empirical evidence suggests that when crystallization was rapid, numerous crystalline lumps lacking a nucleus appeared in all areas of the ma-

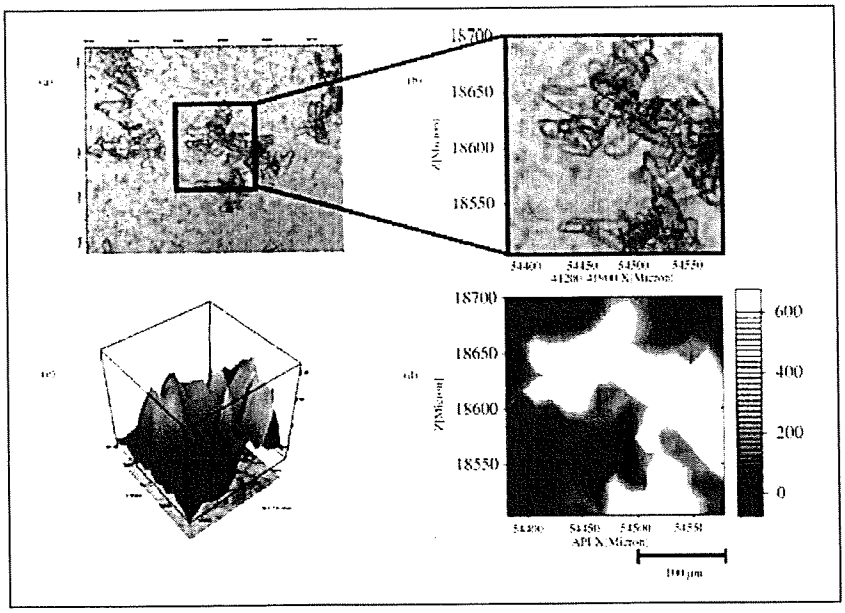

Fig. 4:
Micrographs and Raman chemical maps obtained from the model tape (R-10). a: Micrograph of a 600 × 500 µm area, b: Enlarged micrograph of a 200 × 200 µm area, c: 3D Raman chemical map that corresponds with that in d, d: Raman chemical map that corresponds with b. The distribution of the TBR crystals in the matrix was clearly detected by both methods

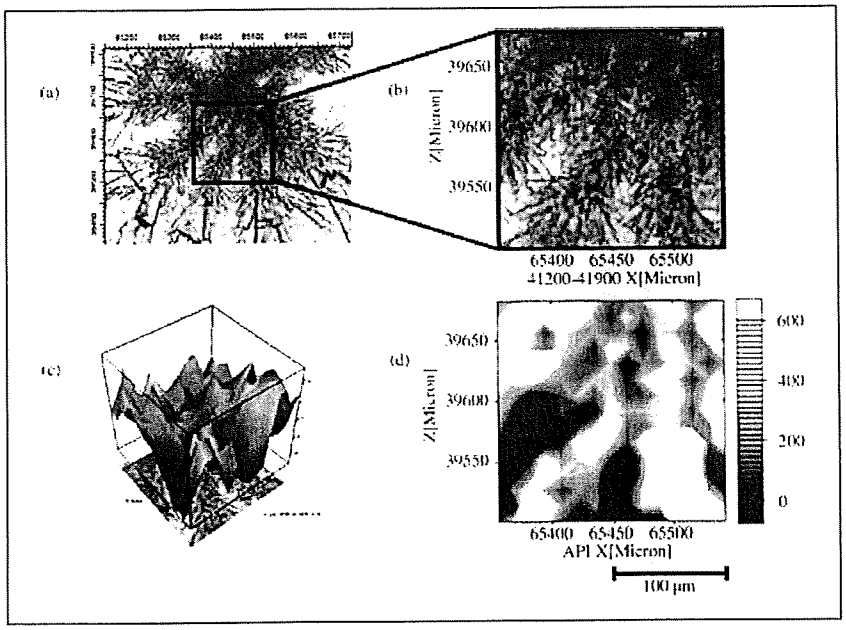

Fig. 5:
Micrographs and Raman chemical maps obtained from the model tape (A-20). a: Micrograph of a 600 × 500 µm area, b: Enlarged micrograph of a 200 × 200 µm area, c: 3D Raman chemical map that corresponds with d, d: Raman chemical map that corresponds with b. The mass of the crystals, with radiating branches, was observed in the matrix. The Raman chemical map of TBR corresponding to the micrograph was obtained

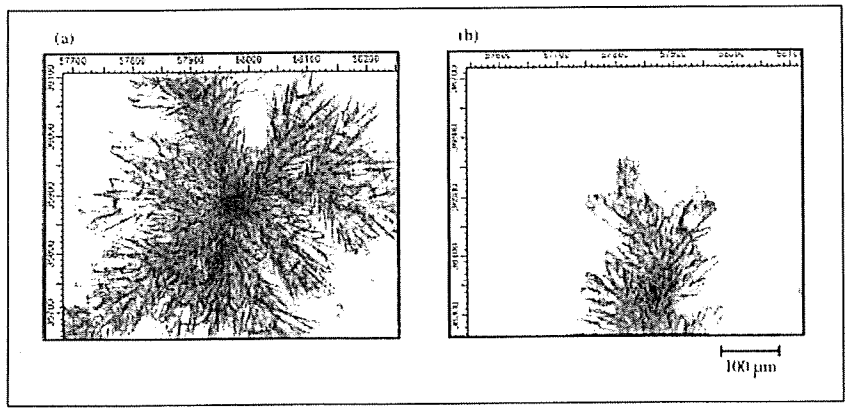

Fig. 6:
Micrographs of the mass of TBR crystals obtained from A-20. a: Core with radiating branches, b: Top of the branch. Pillar-shaped crystals generated successively at the top of branches were observed microscopically

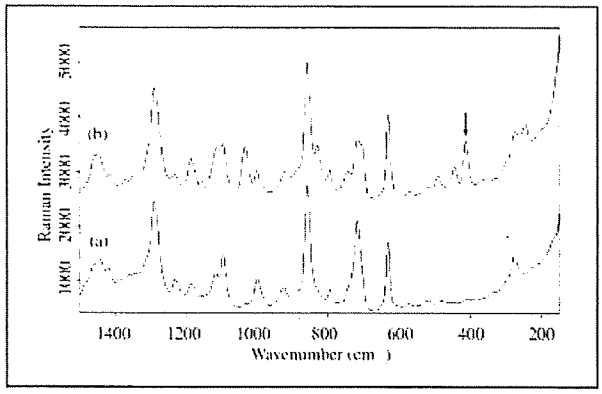

Fig. 7: Raman spectra of commercial tape. a: Background, b: The area where crystals were observed. The characteristic peak (415 cm^{-1}) of TBR was detected

trix, but in cases of slow crystallization, crystals formed around a nucleus. An empirical understanding of such processes would also suggest that the TBR crystals formed more rapidly in the rubber matrix than in the acrylic matrix. The processes of crystallization in these matrices agreed with the empirical evidence obtained here. It appears that new crystals will form around a nucleus, because surrounding molecules are stimulated to crystallize by a nucleus, as shown in Fig. 6. Raghavan et al. (2001) reported that the nucleation process depends in such cases on the hydrogen-bonding functional groups of not only the active drug, but also the polymer. Therefore, it appears likely that differences between the polymer structures of matrices contribute to differences in the process of crystal formation in those matrices. Although further study will still be needed to explain this phenomenon, it appears that the growth mechanism of TBR crystals in each matrix

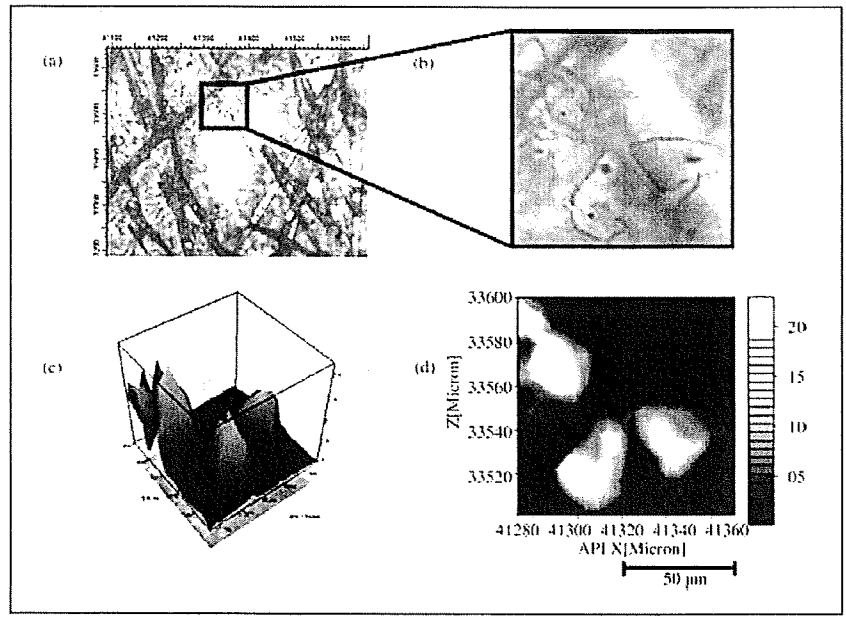

Fig. 8:
Micrographs and Raman chemical maps obtained from the commercial tape (1 mg TBR in the tape). a: Micrograph of a 570 × 450 µm area, b: Enlarged micrograph of a 100 × 100 µm area, c: 3D Raman chemical map that corresponds with d, d: Raman chemical map that corresponds with b. TBR crystals were clearly detected in the matrix

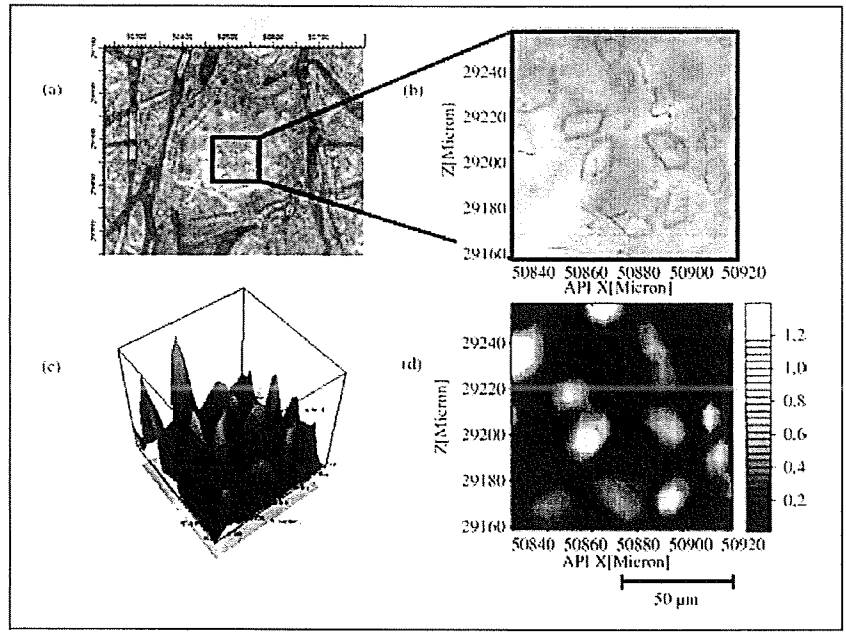

Fig. 9:
Micrographs and Raman chemical maps obtained from commercial tape (2 mg TBR in tape). a: Micrograph of a 570 × 450 µm area, b: Enlarged micrograph of a 100 × 100 µm area, c: 3D Raman chemical map that corresponds with d, d: Raman chemical map that corresponds with b. The crystal distribution suggested that rubber matrix was used for these products

may depend in part on hydrogen bonding between functional groups of TBR and the polymer.

2.5. Analysis of commercial products using MLRSM

MLRSM was used here to detect TBR crystals in commercial products. In these samples, there was a supporting board made of cloth, and a liner made of a white, plastic-like material. The tapes were measured after the liner was removed. Figure 7 shows the Raman spectra of commercial tape. Figure 7a or b were obtained from the area where crystals were not observed or the area where crystals were observed, respectively. The characteristic peak of TBR at 415 cm^{-1} was detected. Figures 8 and 9 show the micrographs (a and b) and the Raman chemical maps (c and d) obtained from the commercial product, Hokunalin® tape, examined in 1 mg and 2 mg sizes, respectively. Areas in which TBR crystals were observed were selected for obtaining the Raman chemical maps. In both micrographs, more crystals appeared to be present in the 2 mg tape than in the 1 mg tape. However, according to the documentation for this product, several sizes of tape, prepared by cutting sections from a larger sheet, can yield various products. Therefore, the TBR content in a particular unit area in several types of Hokunalin® tapes will remain equivalent. It has been hypothesized that the number of crystals in a measured area is affected by the area selected for mapping. Moreover, TBR crystals were also observed that did not assume the lump-shaped formation in this product. Round, pillar-shaped crystals ranging in size from 6×15 μm to 30×40 μm were also observed. The formation of TBR crystals in the product was similar to that observed in a model tape made of a rubber matrix. Helpful information was provided in the attached documentation regarding the medical additives (e.g., polyisobutylene, polybutene, and lipocyclic petroleum resin) used to prepare the rubber matrix. The results of the present study suggest that the crystal formation patterns in a matrix yield useful information about unique matrix characteristics.

3. Discussion

The application of MLRSM to detect the crystals of an active drug in transdermal tapes has been studied. In the case of these TDDS pharmaceutical products, microscopy and chemical mapping method were useful for evaluating the quality of these products as non-destructive spectroscopic technology. Moreover, MLRSM could be used to measure products equipped with a liner for the purpose of quality control during processing, as well as to assess the crystallization of an active drug during storage. Non-destructive spectroscopic methods may be used for analysis of the chemical state and distribution of an active drug, not only in the case of transdermal tapes, but also in film-form products in pharmaceutical development. Furthermore, these methods could be applied as analytical tools to evaluate various factors affecting product quality in the manufacturing process.

4. Experimental

4.1. Microscopic Laser Raman Spectroscopy and Mapping (MLRSM) instrument and measurement conditions

MLRSM measurement was performed using the SENTERRA Dispersive Raman Microscope (Bruker Optics K.K., Germany). Excitation wavelength, laser power, integration time, number of scans, spatial resolution and grating were set at 785 nm, 100 mW, 10 s, 1 scan, 2 μm and 1200 lines/mm, respectively.

4.2. Materials

Tulobuterol (TBR, purity > 99.0%) was provided by Hisamitsu Pharmaceutical Co., Inc. (Tokyo, Japan). 2-Ethylhexyl acrylate vinylpyrrolidone copolymer, isopropyl myristate, polyisobutylene, polybutene, and lipocyclic petroleum resin for matrices of model patches were used as Japanese Pharmaceutical Excipients (JPE)-quality products. Hokunalin® Tape (1 mg and 2 mg) (Maruho Co. Ltd., Osaka, Japan) were purchased from a commercial source.

4.3. Preparation of model tapes

Model tapes were prepared by the TDDS Laboratory, Hisamitsu Pharmaceutical Co., Inc. (Tsukuba, Japan). In order to identify crystalline lumps of TBR in the matrix, two types of matrix, rubber and acrylic, were prepared. TBR and other matrix adhesive solution ingredients were mixed and thoroughly stirred. The mixture was extended on a liner and residual solvents were removed by drying. The matrix was adjusted to a constant thickness (approximately 50 μm) and pasted onto a supporting board. A polyethylene terephthalate (PET) film was selected for the liner and the supporting board of the model tapes. Then, the sample was cut to a size of 36 mm diameter. TBR crystals in the model tapes were generated by leaving the sample to stand for one week (a rubber matrix) or one month (an acrylic matrix).

Model tapes were prepared that contained 0w/w% (R-0, placebo), and 10 w/w% (R-10) of TBR in a rubber matrix that consisted of polyisobutylene, polybutene, and lipocyclic petroleum resin. Small white crystals were seen in all areas of the matrix in the R-10 sample. Model tapes were prepared that contained 0 w/w% (A-0, placebo) and 20 w/w% (A-20) of TBR in an acrylic matrix composed of acrylic adhesive polymer and isopropyl myristate. Due to the solubility of TBR, higher TBR concentrations were necessary to generate crystals in the acrylic matrix than in the rubber matrix.

4.4. Measurement of model tapes and commercial products

The model tapes with the liner were placed on a measurement stand with the liner side facing up. For the measurement of the model tapes, micrographs were obtained and chemical mapping was performed by microscopically focusing on crystals of interest. For the MLRSM measurements of the commercial TBR transdermal tapes, the tapes were placed without the liner on the measurement stand, with the adhesive side facing up.

Acknowledgement: This study was supported in part by a research grant from the Ministry of Health, Labour and Welfare (H17-iyaku-ippan-040).

References

Deely C, Spragg R, Threlfall T (1991) A Comparison of Fourier transform infrared and near-infrared Fourier transform Raman spectroscopy for quantitative measurements: an application in polymorphism. Spectrochim Acta 47: 1217–1223.

Falcon J, Berglund K (2004) In situ monitoring of antisolvent addition crystallization with principal components analysis of Raman spectra. Cryst Growth Des 4: 457–463.

Ferrari E, Davey R (2004) Solution-mediated transformation of α to β l-glutamic acid: rate enhancement due to secondary nucleation. Cryst Growth Des 4: 1061–1068.

Findlay P, Bugay D (1998) Utilization of Fourier transform-Raman spectroscopy for the study of pharmaceutical crystal forms. J Pharm Biomed Anal 16: 921–930.

Horiguchi T, Kondo R, Miyazaki J, Torigoe H, Tachikawa S (2004) Clinical evaluation of tulobuterol patch in patients with mild or moderate persistent bronchial asthma-effects of long-term treatment on airway inflammation and hypersensitivity. Nihon Kokyuki Gakkai Zasshi 42: 132–137.

Hu Y, Liang J, Myerson A, Taylor LS (2005) Crystallization monitoring by Raman spectroscopy: simultaneous measurement of desupersaturation profile and polymorphic form in flufenamic acid systems. Ind Eng Chem Res 44: 1233–1240.

Iikura Y, Uchiyama H, Akimoto K, Ebisawa M, Sakaguchi N, Tsubaki T, Ishizu H, Kabayama H, Yagi K, Miura K (1995) Pharmacokinetics and pharmacodynamics of the tulobuterol patch, HN-078, in childhood asthma. Ann Allergy Asthma Immunol 74: 147–151.

Langkilde F, Sjöblom J, Tekenbergs-Hjelte L, Mrak A (1997) Quantitative FT-Raman analysis of two crystal forms of a pharmaceutical compound. J Pharm Biomed Anal 15: 687–696.

Murphy BM, Prescott SW, Larson I (2005) Measurement of lactose crystallinity using Raman spectroscopy. J Pharm Biomed Anal 38: 186–190.

Nørgaard L, Hahn MT, Knudsen LB, Farhat IA, Engelsen SB (2005) Multivariate near infrared and Rama spectroscopic quantifications of the crystallinity of lactose in whet permeate powder. Int Dairy J 15: 1261–1270.

Ono T, ter Horst J, Jansens P (2004) Quantitative measurement of the polymorphic transformation of l-glutamic acid using in-situ Raman spectroscopy. Cryst Growth Des 4: 465–469.

Raghavan SL, Trividic A, Davis AF, Hadgraft J (2001) Crystallization of hydrocortisone acetate: influence of polymers. Int J Pharm 212: 213–221.

Schöll J, Bonalumi D, Vicum L, Mazzotti M (2006) In situ monitoring and modeling of the solvent-mediated polymorphic transformation of l-glutamic acid. Cryst Growth Des, 6: 881–891.

Starbuck C, Spartails A, Wai L, Wang J, Fernandez P, Lindemann C, Zhou G, Ge Z (2002) Process optimization of a complex pharmaceutical polymorphic system via in situ Raman spectroscopy. Cryst Growth Des 2: 515–522.

Taylor LS, Zografi G (1998) Quantitative analysis of crystallinity using FT-Raman spectroscopy. Pharm Res 15: 755–761.

Uematsu T, Nakano M, Kosuge K, Kanamaru M, Nakashima M (1993) The pharmacokinetics of the beta 2-adrenocepter agonist, tulobuterol given transdermally and by inhalation. Eur J Clin Pharmacol 44: 361–364.

Wang F, Wachter J, Antosz F, Berglund K (2000) An investigation of solvent-mediated polymorphic transformation of progesterone using in situ Raman spectroscopy. Org Proc Res Dev, 4: 391–395.

AAPS PharmSciTech, Vol. 10, No. 2, June 2009 (© 2009)
DOI: 10.1208/s12249-009-9243-0

Research Article

Near-Infrared Analysis of Hydrogen-Bonding in Glass- and Rubber-State Amorphous Saccharide Solids

Ken-ichi Izutsu,[1,2] Yukio Hiyama,[1] Chikako Yomota,[1] and Toru Kawanishi[1]

Received 17 October 2008; accepted 9 April 2009; published online 7 May 2009

Abstract. Near-infrared (NIR) spectroscopic analysis of noncrystalline polyols and saccharides (e.g., glycerol, sorbitol, maltitol, glucose, sucrose, maltose) was performed at different temperatures (30–80°C) to elucidate the effect of glass transition on molecular interaction. Transmission NIR spectra (4,000–12,000 cm^{-1}) of the liquids and cooled-melt amorphous solids showed broad absorption bands that indicate random configuration of molecules. Heating of the samples decreased an intermolecular hydrogen-bonding OH vibration band intensity (6,200–6,500 cm^{-1}) with a concomitant increase in a free and intramolecular hydrogen-bonding OH group band (6,600–7,100 cm^{-1}). Large reduction of the intermolecular hydrogen-bonding band intensity at temperatures above the glass transition (T_g) of the individual solids should explain the higher molecular mobility and lower viscosity in the rubber state. Mixing of the polyols with a high T_g saccharide (maltose) or an inorganic salt (sodium tetraborate) shifted both the glass transition and the inflection point of the hydrogen-bonding band intensity to higher temperatures. The implications of these results for pharmaceutical formulation design and process monitoring (PAT) are discussed.

KEYWORDS: amorphous; glass transition; hydrogen-bonding; NIR; PAT.

INTRODUCTION

The development of amorphous solid pharmaceutical formulations requires thorough characterization of physical properties (1–4). Optimizing the molecular mobility and the system viscosity, which both change significantly at glass transition temperature (T_g), is essential to ensure their unique functional characters (e.g., faster dissolution of active ingredients, stabilization of lyophilized protein conformation) and storage stability of these solids. Understanding how the molecular interactions, particularly hydrogen-bonding, in amorphous carbohydrate solids affect their physical properties is relevant to the formulation design and process control (5).

Near-infrared (NIR) spectroscopy is an advancing analytical method that provides varied information on the chemical and physical properties of pharmaceutical formulations including molecular structure, crystallinity (6–8), crystal polymorphs (9,10), residual water content (11), component miscibility (12), protein secondary structure (13), and molecular interactions (14–17). Relatively low absorbance that enables diffuse-reflection measurement and recent advances in chemometrics (e.g., principal component analysis [PCA], partial least-squares calibration [PLS]) make the NIR spectroscopy a powerful nondestructive process analytical tool for quality control (PAT) (18). The applicability of vacuum-sealed samples in glass vials should be an apparent advantage of NIR in the analysis of physically unstable amorphous solids. Proper use of NIR spectroscopy, combined with other sophisticated in-, on-, and at-line analytical tools (e.g., mid-infrared, far-infrared, terahertz, and Raman spectroscopy; thermal analysis), should improve the product and process understanding required for better formulation quality (16,19,20).

The purpose of this study was to characterize hydrogen-bonding profiles in rubber- and glass-state amorphous solids by NIR spectroscopy. The random configuration of molecules and the accompanying wide variation of molecular interactions in amorphous polyol and saccharide solids provide broad absorption bands in the NIR spectra (6,7). Some of the broad bands (e.g., OH stretching vibration) indicate different hydrogen-bonding states (e.g., intermolecular, intramolecular, free) in the solids (21,22). The profiles of the hydrogen-bonding in water and some alcohol liquids depend largely on temperature (23–25). Recent mid-infrared studies on the amorphous saccharide films indicate different temperature-dependent shifts of OH stretching (3,300–3,400 cm^{-1}) and bending (1,000–1,100 cm^{-1}) vibration band peaks between their glass (below T_g) and rubber (above T_g) states (26,27). It is plausible that NIR spectroscopy provides valuable information on the molecular interactions and physical properties of various noncrystalline samples (e.g., liquid, rubber-state solid, glass-state solid).

[1] National Institute of Health Sciences, Kamiyoga 1-18-1, Setagaya, Tokyo 158-8501, Japan.
[2] To whom correspondence should be addressed. (e-mail: izutsu@nihs.go.jp)

MATERIALS AND METHODS

Materials

All chemicals employed in this study were of analytical grades and were obtained from the following commercial sources: glycerol and sorbitol (Wako Pure Chemical, Osaka, Japan); maltose monohydrate, sucrose, and sodium tetraborate (Sigma Chemical, St. Louis, MO, USA); deuterium water (Acros Organics, Geel, Belgium); maltitol and maltotriitol (Hayashibara Biochemical Laboratories, Okayama, Japan).

Preparation of Freeze-Dried Amorphous Solids

Freeze-dried solids were prepared by lyophilizing aqueous polyol and saccharides solutions (100 mg/mL, 2 mL) in flat-bottom borosilicate glass vials (21 mm diameter; SVF-10, Nichiden-rika Glass, Kobe, Japan) using a Freezevac-1C freeze-drier (Tozai Tsusho, Tokyo, Japan). The sample solutions frozen by immersion in liquid nitrogen were dried under vacuum without temperature control for 16 h and then maintained on the shelf at 35°C for 8 h. Hydrogen/deuterium-exchanged glycerol, sorbitol, and glucose were obtained by freeze-drying the solutions in D_2O twice (200 mg/mL).

Preparation of Cooled-Melt Amorphous Solids

The cooled-melt solids subjected to thermal and NIR analysis were obtained by melting the crystalline powder in a quartz cuvette (1-mm light path length; Starna Optiglass, Hainault, UK) or small borosilicate glass tubes (approximately 4 mm internal diameter; TGK, Tokyo, Japan) in a drying oven (DP23, Yamato Scientific, Tokyo, Japan) at 200°C (sucrose) or 180°C (other saccharides) under vacuum for 20 min, then cooled at room temperature. Amorphous maltose solids were prepared from the monohydrate crystal with (dehydrated) or without (partially hydrated) vacuum-drying. The cooled-melt solids without apparent crack or bubbles were subjected to the following transmission NIR analysis.

Thermal Analysis

A differential scanning calorimeter (DSC Q-10, TA Instruments, New Castle, DE, USA) and software (Universal Analysis 2000, TA Instruments) were used to obtain the thermal properties of the amorphous solids. Solids (2–5 mg) in hermetic aluminum cells were scanned from −30°C at 5°C/min under N_2 gas flow. Glass transition temperatures were determined from the maximum inflection point of the discontinuities in the heat flow curves.

NIR Spectroscopy

NIR analysis was performed using a FT-NIR system (MPA, Bruker Optik, Germany) equipped with a sample temperature controller and OPUS software. Transmission NIR spectra of liquids and cooled-melt amorphous solids were obtained from 30°C to 80°C at every 5°C with 5-min intervals between the measurements. Absorbance in the 12,000 to 4,000 cm^{-1} range was obtained with a 2-cm^{-1} resolution in 128 scans. The absorbance of air was subtracted as background. The NIR spectra were baseline-corrected in the 8,000–9,000 cm^{-1} range and smoothed at 25 points. The possible effect of a temperature-induced solid volume change was not compensated in this study. Diffuse-reflection NIR spectra of crystal powders and freeze-dried solids in cylindrical borosilicate glass vials were obtained from the bottom of the container at room temperature.

RESULTS

Figure 1 shows the diffuse-reflection NIR spectra of mannitol, maltose monohydrate, sucrose, glucose, and sorbitol in different physical states (crystalline powder, freeze-dried solid) obtained noninvasively from the bottoms of the glass vials. The crystalline powders showed several unique sharp bands of OH and CH vibrations in the overtone (5,000–7,500 cm^{-1}) and combination (4,000–5,000 cm^{-1}) spectral regions. The absorbance of water in the maltose monohydrate crystal (around 5,150 cm^{-1}) disappeared by lyophilization. Freeze-dried amorphous sucrose and maltose solids showed broad absorption bands that indicate diversified interactions between the spatially less-ordered molecules. Contrarily, some sharp peaks (e.g., 4,375 cm^{-1}) indicated partial crystallinity of the freeze-dried mannitol (4,28). Thermal analysis of the freeze-dried solids also indicated different component crystallinity (data not shown). Freeze-drying of glucose and sorbitol resulted in collapsed solids, which spectra varied largely between the vials (data not shown). Amorphous saccharide solids prepared by cooling the heat-melt also showed varied diffuse-reflection NIR spectra.

Transmission NIR analysis of cooled-melt amorphous solids (e.g., sorbitol, glucose) and a liquid (glycerol) in a quartz cell (1-mm light path length, 30°C) showed similar spectra with some broad bands (Fig. 2A). The large bands in

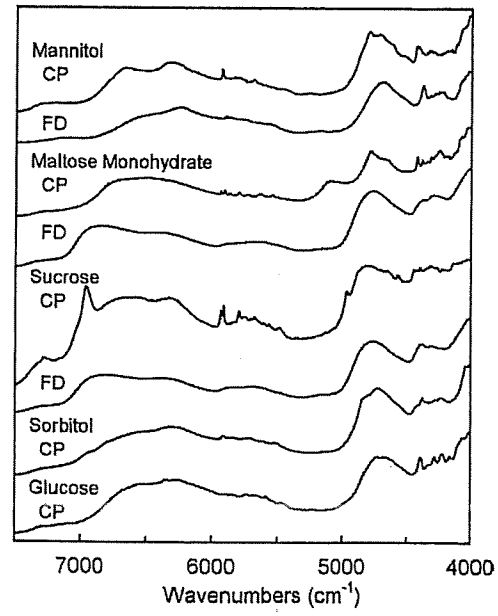

Fig. 1. Diffuse-reflection NIR spectra of crystalline powder (*CP*) and freeze-dried solid (*FD*) containing sugars and sugar alcohols obtained at the bottoms of glass vials

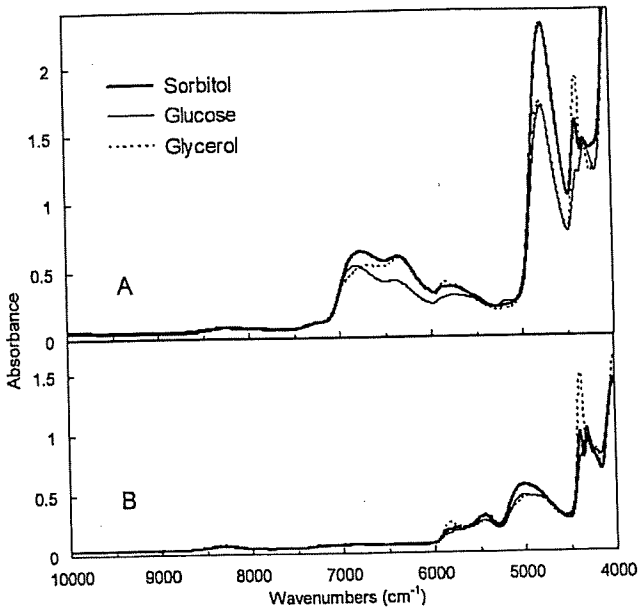

Fig. 2. Transmission NIR spectra of liquid (glycerol) and cooled-melt solids (sorbitol, glucose) in a quartz cell (1-mm light path length) prepared with **A** without and **B** with hydrogen/deuterium exchange (30°C)

the overtone spectral region represent OH stretching vibration first overtones of intermolecular hydrogen-bonding groups (6,200–6,500 cm^{-1}) and intramolecular or nonhydrogen-bonding groups (6,600–7,100 cm^{-1}) (21,22,25). The addition of H_2O (2–10%, *w/w*) to glycerol increased the absorbance at around 4,110, 5,152, and 6,925 cm^{-1} in the NIR spectra (data not shown). Hydrogen/deuterium-exchanged samples showed a large band that suggested an OD stretching vibration at around 5,000 cm^{-1} (Fig. 2B) (23). Lower absorbance of the hydrogen/deuterium-exchanged amorphous solids at 6,000–7,100 cm^{-1} confirmed the significance of the OH stretching vibration band in the spectral region. Thermal analysis showed that the cooled-melt sorbitol (T_g=−1.2°C) and glucose (T_g= 45.8°C) are in the rubber and glass states, respectively, at 30°C.

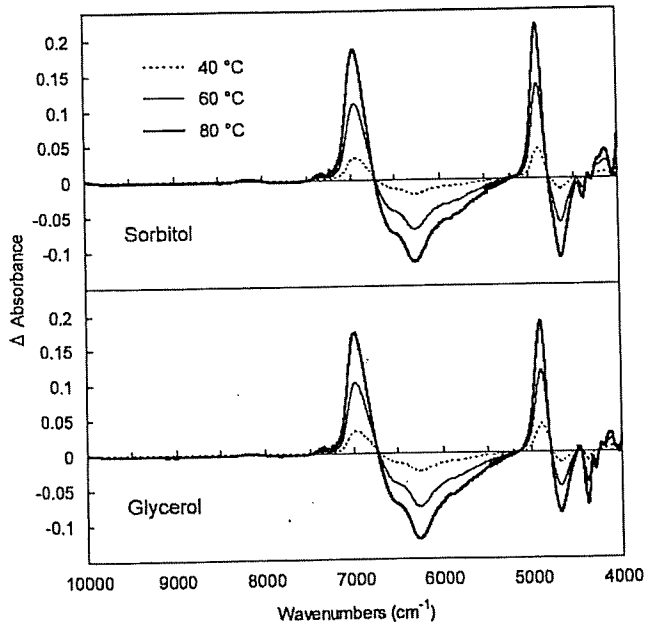

Fig. 3. Effect of heating on the transmission NIR spectra of glycerol liquid and cooled-melt sorbitol solid (1-mm light path length). Difference spectra were obtained by subtracting the absorbance of the samples at 30°C

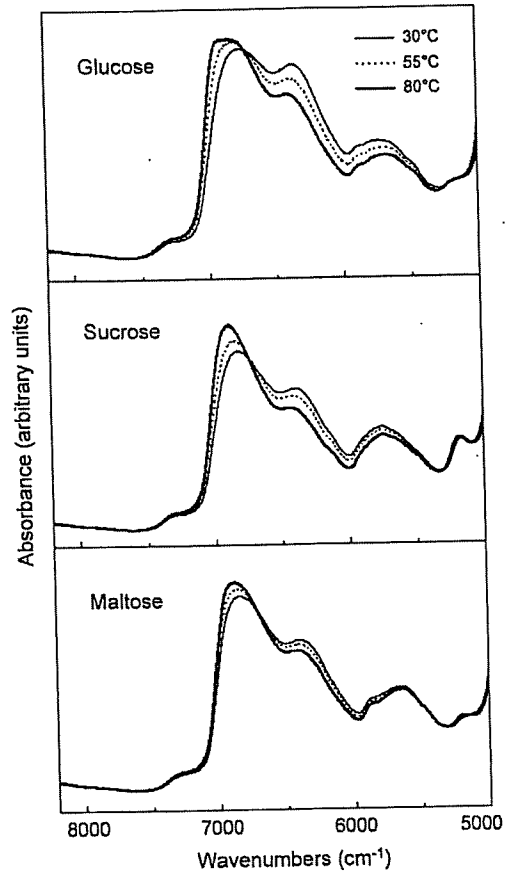

Fig. 4. Transmission NIR spectra of cooled-melt amorphous glucose, sucrose, and maltose (dehydrated) solids in glass tubes (approximately 4 mm interior diameter) obtained at 30°C, 55°C, and 80°C

The effect of heating on the transmission NIR spectra of the noncrystalline sorbitol and glycerol are shown as the difference spectra (Fig. 3). The changes indicated the shift of the major bands at 6,000–7,000 cm^{-1} (OH stretching vibration first overtone) and at around 4,750 cm^{-1} (OH stretching/bending combination) in the original spectra to higher wave numbers at the elevated temperatures (40°C, 60°C, and 80°C). The apparent decrease in the absorbance at 6,000–6,500 cm^{-1} and the concomitant absorbance increase at 6,700–7,100 cm^{-1} suggested heat-induced changes in the hydrogen-bonding profiles of the OH groups from intermolecular to intramolecular or free bonds.

Transmission NIR spectra (overtone region) of cooled-melt glucose, sucrose, and maltose (dehydrated) obtained at different temperatures (30°C, 55°C, and 80°C) suggested varied heat-induced changes in the hydrogen-bonding band intensity (Fig. 4). The larger spectral change observed in the lower glass transition temperature solids (glucose=45.8°C) suggested the contribution of the different hydrogen-bonding profiles to the physical properties. The solids were prepared

in small glass tubes (approximately 4 mm internal diameter) to prevent crack formation in the cooling process. The browning of sucrose during the preparation indicated its partial degradation at high temperatures. A small absorption band at 5,150 cm^{-1} suggested residual water in the amorphous saccharide solids. Relatively large absorbance at the 6,200- to 6,500-cm^{-1} region in the amorphous glucose solid suggested a larger contribution of the intermolecular hydrogen-bonding compared to those in other saccharides. Different dehydration process and accompanying changes in the molecular interactions should explain the partially different spectra of the cooled-melt glucose solid prepared in the quartz optical cell (Fig. 2) and the glass tube (Fig. 4).

The relationship between the hydrogen-bonding profiles and the physical states of the amorphous solids were further studied. Thermal analysis showed varied glass transition temperatures of the cooled-melt amorphous polyol and saccharide solids (Table I). The changes in the absorbance of the intermolecular hydrogen-bonding OH band peak (6,200–6,500 cm^{-1}) obtained every 5°C were plotted in Fig. 5. The spectral region was chosen for comparison because of the smaller overlapping absorbance of residual water compared to that in the intramolecular hydrogen-bonding band region (6,600–7,100 cm^{-1}) (11). The noncrystalline samples showed three types of intermolecular hydrogen-bonding band intensity changes depending on their glass transition temperatures. A rubber-state solid (sorbitol, T_g=−1.2°C) and glycerol liquid showed relatively large (<0.04 U/5°C) band intensity drops from the lowest measurement temperature. Contrarily, amorphous dehydrated maltose that remained in the glass state throughout the measurement temperature range (80°C< T_g) showed a much smaller band intensity change. Other solids (e.g., glucose, sucrose, maltotriitol; 30°C< T_g<80°C) showed larger declines of the band intensity above their glass transition temperatures. Plotting of the band intensity against the temperature showed apparent inflection at the glass transition. Plateau of the plot above the T_g should indicate large and constant temperature-dependent reduction of the molecular interactions similar to that of molecular liquids.

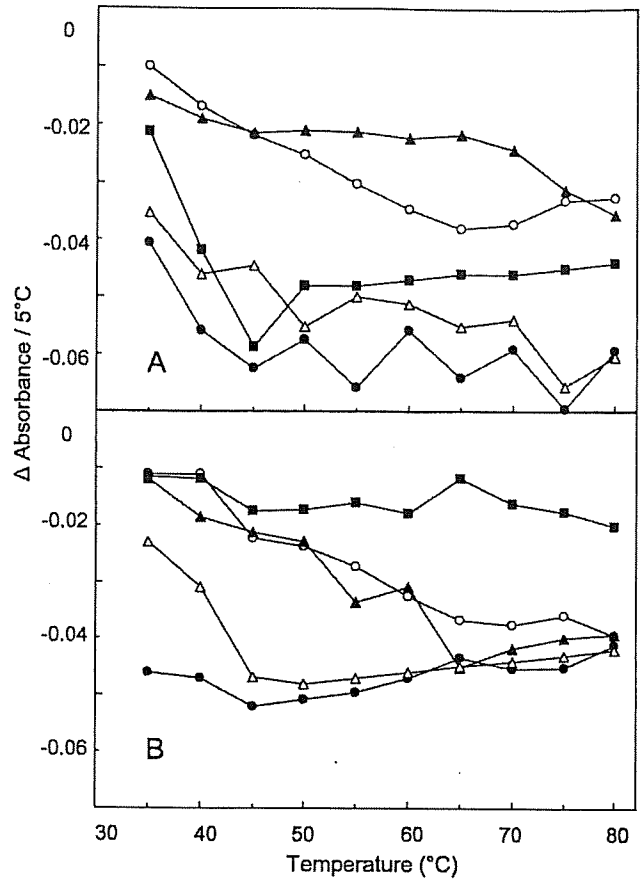

Fig. 5. Changes in the absorbance of intermolecular hydrogen-bonding OH vibration band obtained by transmission NIR scan of noncrystalline samples at 5°C intervals. Each point of the curves represents the mean of duplicated measurements. Each symbol denotes **A** glycerol (*filled circles*), sorbitol (*open triangles*), glucose (*filled squares*), sucrose (*open circles*), maltotriitol (*filled triangles*) and **B** maltose (*filled squares*), maltose hydrate (*open circles*), and maltose+sorbitol at the weight ratios of 2:1 (*filled circles*), 3:1 (*open triangles*), and 5:1 (*filled triangles*)

Table I. Glass Transition Temperature of Cooled-Melt Amorphous Solids

Glass transition temperatures	
Maltose	99.4±1.2
Maltotriitol	79.5±0.8
Maltose (w/o vacuum-drying)	62.6±1.7
Sucrose	57.9±3.2
Maltitol	49.3±0.5
Glucose	45.8±2.2
Glycerol (liquid)	n.d.
Sorbitol	−1.2±0.9
Maltose+sorbitol 5:1[a]	66.5±1.9
Maltose+sorbitol 3:1[a]	48.6±0.5
Maltose+sorbitol 2:1[a]	31.0±0.3
Maltitol+$Na_2B_4O_7$ 40:1[b]	59.0±2.1
Maltitol+$Na_2B_4O_7$ 25:1[b]	69.2±1.7

Data are presented as mean±SD (n=3)
[a] Weight ratio
[b] Molar ratio

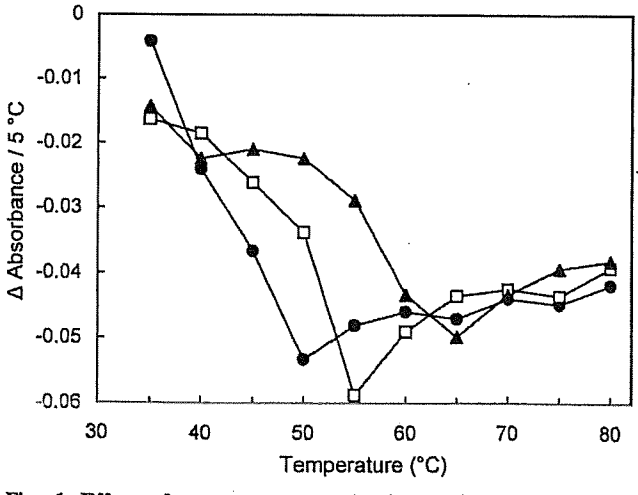

Fig. 6. Effect of temperature on the intermolecular hydrogen-bonding OH vibration band absorbance of maltitol (*filled circles*) and its mixture with $Na_2B_4O_7$ at the molar ratio of 40:1 (*open squares*) and 25:1 (*filled triangles*) obtained at 5°C intervals (n=2)

Some solids containing multiple components also showed larger heat-induced reduction of the intermolecular hydrogen-bonding band in the rubber state. The mixing of components (e.g., maltose and sorbitol) or higher residual water (e.g., cooled-melt maltose monohydrate prepared without vacuum-drying) shifts the glass transition temperature of the amorphous solids (Table I). These solids showed larger heat-induced intermolecular hydrogen-bonding band intensity reductions at above their glass transition temperatures (Fig. 5). Some inorganic salts (e.g., sodium phosphates, sodium citrates) affect the glass transition temperature of amorphous polyol and saccharide solids (29,30). The addition of a small amount of sodium tetraborate ($Na_2B_4O_7$) significantly raised the T_g of cooled-melt maltitol solids (Table I), as well as the inflection temperature of the intermolecular hydrogen-bonding band intensity (Fig. 6) (31,32).

DISCUSSION

The NIR study showed varied hydrogen-bonding states of OH groups in the noncrystalline polyol and saccharide solids that depended both on their temperatures and their physical states (glass and rubber). The heating-induced reduction of the intermolecular hydrogen bond was consistent with the literature on the NIR analysis of water, alcohol, and polyol liquids (25,33). The limited absorbance of hydrogen/deuterium-exchanged polyols (glucose, sorbitol) at above 6,000 cm^{-1} indicated the contribution of readily exchangeable OH groups to the temperature-dependent band intensity change. The appropriate sample temperature control and the constant light path length made the transmission NIR measurement suitable to study the relationship between the physical states and the molecular interactions. The general trends observed in the transmission mode should be basically applicable to other data detection modes (e.g., diffuse-reflection).

The glass transition of the amorphous solids did not directly affect the NIR spectra, but it altered the extent of the heat-induced hydrogen-bonding band intensity change. The result was in agreement with the different temperature-dependent changes in the mid-infrared OH stretching and bending band peak positions of saccharide films in the glass and rubber states (26,27). Loosening of the intermolecular hydrogen-bonding network should induce the higher molecular mobility and lower viscosity of the rubber-state amorphous solids. The rubber-state amorphous solids are, from another physical perspective, deeply supercooled liquids with extremely high viscosity. The similarity in physical states would explain the large constant heat-induced reduction of the intermolecular band intensity in the polyol liquids (e.g., glycerol) and the rubber-state solids. The smaller heat-induced spectral changes below the T_g would increase the mobility of molecules, leading to slow but not negligible temperature-dependent chemical degradation and/or ingredient crystallization in the long-term storage of the glass-state amorphous solids (34). Further assignment of the bands in the NIR spectra and mathematical data processing should increase the relevance of the analysis.

Information on the molecular interactions (e.g., hydrogen-bonding) that determine the physical properties should be relevant for the rational design of amorphous formulations. NIR spectroscopy should be used to characterize the molecular interactions in certain multicomponent amorphous systems containing the active pharmaceutical ingredients, excipients (e.g., stabilizer, pH modifier), and residual water. The availability of several detection modes that involve samples in glass containers without exposure to unfavorable environments (e.g., humid atmosphere) is a major advantage of NIR spectroscopy over other analytical methods for the characterization of the amorphous freeze-dried formulations (15). The proper choice of excipients that form and/or induce intermolecular hydrogen-bonding (e.g., disaccharides, sodium phosphate) should provide the storage stability and functional properties required for the amorphous formulations.

NIR spectroscopy is a powerful analytical tool for process monitoring and raw material inspection (18,20). Ensuring chemical and physical properties during the process is important to obtain reliable pharmaceutical formulations. Clinical functions and storage stabilities of the amorphous solid formulations depends not only on their glass transition temperatures (T_g) but also on other physical characters (e.g., residual crystallinity, structural relaxation) that are affected by process parameters (e.g., thermal history) (3). Several mathematical data processing methods, including PLS and PCA, have been used to obtain information on the chemical and physical properties of solids (e.g., crystallinity, collapse, residual water, chemical degradation) from the NIR spectra. The preparation of amorphous solids often includes low (e.g., freeze-drying) or high (e.g., melting, extrusion) temperature processes. Understanding the effect of temperature and physical states on the NIR spectra, as well as appropriate data compensation, should increase the relevance of the sophisticated analytical methods.

ACKNOWLEDGEMENT

The present study was supported by the Japan Health Sciences Foundation (KH31029, KHB1006).

REFERENCES

1. Cui Y. A material science perspective of pharmaceutical solids. Int J Pharm. 2007;339:3–18.
2. Hancock BC, Zografi G. Characteristics and significance of the amorphous state in pharmaceutical systems. J Pharm Sci. 1997;86: 1–12.
3. Hilden LR, Morris KR. Physics of amorphous solids. J Pharm Sci. 2004;93:3–12.
4. Nail SL, Jiang S, Chongprasert S, Knopp SA. Fundamentals of freeze-drying. Pharm Biotechnol. 2002;14:281–360.
5. Tang XC, Pikal MJ, Taylor LS. The effect of temperature on hydrogen bonding in crystalline and amorphous phases in dihydropyrine calcium channel blockers. Pharm Res. 2002;19: 484–90.
6. Yonemochi E, Inoue Y, Buckton G, Moffat A, Oguchi T, Yamamoto K. Differences in crystallization behavior between quenched and ground amorphous ursodeoxycholic acid. Pharm Res. 1999;16:835–40.
7. Hogan SE, Buckton G. The application of near infrared spectroscopy and dynamic vapor sorption to quantify low amorphous contents of crystalline lactose. Pharm Res. 2001;18: 112–6.
8. Seyer JJ, Luner PE, Kemper MS. Application of diffuse reflectance near-infrared spectroscopy for determination of crystallinity. J Pharm Sci. 2000;89:1305–16.
9. Otsuka M, Kato F, Matsuda Y. Comparative evaluation of the degree of indomethacin crystallinity by chemoinfometrical Four-

ier-transformed near-infrared spectroscopy and conventional powder X-ray diffractometry. AAPS PharmSci. 2000;2:E9.
10. Tudor AM, Church SJ, Hendra PJ, Davies MC, Melia CD. The qualitative and quantitative analysis of chlorpropamide polymorphic mixtures by near-infrared Fourier transform Raman spectroscopy. Pharm Res. 1993;10:1772–6.
11. Stein HH, Ambrose JM. Near-infrared method for determination of water in aluminum aspirin. Anal Chem. 1963;35:550–2.
12. Jovanović N, Gerich A, Bouchard A, Jiskoot W. Near-infrared imaging for studying homogeneity of protein–sugar mixtures. Pharm Res. 2006;23:2002–13.
13. Bai S, Nayar R, Carpenter JF, Manning MC. Noninvasive determination of protein conformation in the solid state using near infrared (NIR) spectroscopy. J Pharm Sci. 2005;94:2030–8.
14. Izutsu K, Fujimaki Y, Kuwabra A, Aoyagi N. Effect of counterions on the physical properties of L-arginine in frozen solutions and freeze-dried solids. Int J Pharm. 2005;301:161–9.
15. Liu J. Physical characterization of pharmaceutical formulations in frozen and freeze-dried solid states: techniques and applications in freeze-drying development. Pharm Dev Technol. 2006;11: 3–28.
16. Räsänen E, Sandler N. Near infrared spectroscopy in the development of solid dosage forms. J Pharm Pharmacol. 2007;59: 147–59.
17. Reich G. Near-infrared spectroscopy and imaging: basic principles and pharmaceutical applications. Adv Drug Deliv Rev. 2005;57: 1109–43.
18. Fevotte G, Calas J, Puel F, Hoff C. Applications of NIR spectroscopy to monitoring and analyzing the solid state during industrial crystallization processes. Int J Pharm. 2004;273:159–69.
19. FDA. Guidance for industry: PAT—a framework for innovative pharmaceutical development, manufacturing and quality assurance. http://www.fda.gov/cder/guidance/6419fnl.htm (2004)
20. De Beer TR, Allesø M, Goethals F, Coppens A, Heyden YV, De Diego HL, et al. Implementation of a process analytical technology system in a freeze-drying process using Raman spectroscopy for in-line process monitoring. Anal Chem. 2007;79:7992–8003.
21. Ozaki Y, Kawata S. Near-infrared spectroscopy. Tokyo: Japan Scientific Societies Press; 1996.
22. Shenk JS, Workman JJ Jr., Westerhaus MO. Application of NIR spectroscopy to agricultural products. In: Burns DA, Ciurczak WW, editors. Handbook of near-infrared analysis. New York: Taylor & Francis; 2001. p. 419–74.
23. Czarnecki MA, Czarnik-Matusewicz B, Ozaki Y, Iwahashi M. Resolution enhancement and band assignments for the first overtone of OH(D) stretching modes of butanols by two-dimensional near-infrared correlation spectroscopy. 3. Thermal dynamics of hydrogen bonding in butan-1-(ol-d) and 2-methylpropan-2-(ol-d) in the pure liquid states. J Phys Chem A. 2000;104:4906–11.
24. Czarnecki MA, Ozaki Y. The temperature-induced changes in hydrogen bonding of decan-1-ol in the pure liquid phase studied by two-dimensional Fourier transform near-infrared correlation spectroscopy. Phys Chem Chem Phys. 1999;1:797–800.
25. Maeda H, Ozaki Y. Near infrared spectroscopy and chemometrics studies of temperature-dependent spectral variations of water: relationship between spectral changes and hydrogen bonds. J Near Infrared Spectrosc. 1995;3:191–201.
26. Wolkers WF, Oldenhof H, Alberda M, Hoekstra FA. A Fourier transform infrared microspectroscopy study of sugar glasses: application to anhydrobiotic higher plant cells. Biochim Biophys Acta. 1998;1379:83–96.
27. Wolkers WF, Oliver AE, Tablin F, Crowe JH. A Fourier-transform infrared spectroscopy study of sugar glasses. Carbohydr Res. 2004;339:1077–85.
28. Cao W, Mao C, Chen W, Lin H, Krishnan S, Cauchon N. Differentiation and quantitative determination of surface and hydrate water in lyophilized mannitol using NIR spectroscopy. J Pharm Sci. 2006;95:2077–86.
29. Ohtake S, Schebor C, Palecek SP, Pablo JJD. Effect of pH, counter ion, and phosphate concentration on the glass transition temperature of freeze-dried sugar–phosphate mixtures. Pharm Res. 2004;21:1615–21.
30. Kets EP, IJpelaar PJ, Hoekstra FA, Vromans H. Citrate increases glass transition temperature of vitrified sucrose preparations. Cryobiology 2004;48:46–54.
31. Miller DP, Anderson RE, de Pablo JJ. Stabilization of lactate dehydrogenase following freeze thawing and vacuum-drying in the presence of trehalose and borate. Pharm Res. 1998;15:1215–21.
32. Izutsu K, Yomota C, Aoyagi N. Inhibition of mannitol crystallization in frozen solutions by sodium phosphates and citrates. Chem Pharm Bull. 2007;55:565–70.
33. Watanabe A, Morita S, Ozaki Y. Temperature-dependent structural changes in hydrogen bonds in microcrystalline cellulose studied by infrared and near-infrared spectroscopy with perturbation-correlation moving-window two-dimensional correlation analysis. Appl Spectrosc. 2006;60:611–8.
34. Yoshioka M, Hancock BC, Zografi G. Crystallization of indomethacin from the amorphous state below and above its glass transition temperature. J Pharm Sci. 1994;83:1700–5.

International Journal of Pharmaceutics 378 (2009) 167–176

Contents lists available at ScienceDirect

International Journal of Pharmaceutics

journal homepage: www.elsevier.com/locate/ijpharm

Pharmaceutical Nanotechnology

Pharmaceutical quality evaluation of lipid emulsions containing PGE_1: Alteration in the number of large particles in infusion solutions

Hiroko Shibata *, Haruna Saito, Chikako Yomota, Toru Kawanishi

National Institute of Health Sciences, Kamiyoga 1-18-1, Setagaya-ku, Tokyo 158-8501, Japan

ARTICLE INFO

Article history:
Received 18 February 2009
Received in revised form 15 April 2009
Accepted 16 May 2009
Available online 22 May 2009

Keywords:
Emulsion
Prostaglandin E_1
Lipid particle
Release
Generics

ABSTRACT

There are two generics of a parenteral lipid emulsion of prostaglandin E1 (PGE_1) (Lipo-PGE_1) in addition to two innovators. It was reported the change from innovator to generic in clinical practice caused the slowing of drip rate and formation of aggregates in the infusion line. Thus, we investigated the difference of pharmaceutical quality in these Lipo-PGE_1 formulations. After mixing with some infusion solutions, the mean diameter and number of large particles were determined. Although the mean diameter did not change in any infusion solutions, the number of large particles (diameter >1.0 μm) dramatically increased in generics with Hartmann's solution pH 8 or Lactec® injection with 7% sodium bicarbonate. Next, we investigated the effect of these infusion solutions on the retention rate of PGE_1 in lipid particles. The retention rate of PGE_1 in these two infusion solutions decreased more quickly than that in normal saline. Nevertheless, there were no significant differences among the formulations tested. Our results suggest that there is no difference between innovators and generics except in mixing with these infusion solutions. Furthermore, that monitoring the number of large particles can be an effective means of evaluating pharmaceutical interactions and/or the stability of lipid emulsions.

1. Introduction

Prostaglandin E1 (PGE_1), which has a strong vasodilatory and antiplatelet activity, is clinically used to treat diseases such as periferal arterial occlusive diseases (Makita et al., 1997; Milio et al., 2003) and ductus arteriosus-dependent congenital heart disease (Kramer et al., 1995). However, PGE_1 has a very short half-life in blood and can elicit various side-effects (Golub et al., 1975; Schramek and Waldhauser, 1989). As a result, a lipid emulsion of PGE_1 (Lipo-PGE_1), in which lipid particles incorporating PGE_1 were coated with lecithin, was developed and applied for clinical treatment in Japan (Mizushima et al., 1983; Otomo et al., 1985). Because the lipid particles are efficiently distributed into the vascular lesion site, Lipo-PGE_1 accumulates in the lesion area and is therefore safer and more effective than free PGE_1 (Mizushima et al., 1990; Mizushima et al., 1983). Indeed, Lipo-PGE_1 is widely used to treat a number of conditions other than arterial occlusive diseases, such as cutaneous ulcer with diabetes and improvement of imaging ability for arterial portography. Two innovator formulations and two generic formulations have already been launched. The composition of each formulation is shown in Table 1. Although generic formulations contain olive oil instead of soybean oil, the other additives are the same as those found in the innovator formulations. Hydrochloric acid or sodium hydrate is added appropriately as a pH adjuster, and the pH of each formulation is adjusted 4.5–6.0.

Lipo-PGE_1 can be intravenously administered by bolus injection, or slowly administered as infusions by mixing with infusion solution. Recently, it was reported that the change from innovator to generic formulation in clinical practice caused the slowing of drip rate and formation of aggregates in the infusion line (Sakaya et al., 2005; Goto et al., 2005). This phenomenon was observed under alkaline conditions in the presence of calcium ions. The Lipo-PGE_1 has an approximate pH of 5. There are some cases where Lipo-PGE_1 is mixed into the infusion solutions of relatively high pH (e.g., Hartmann's solution pH 8; 7% sodium bicarbonate) in order to moderate vascular pain or venous inflammation. Furthermore, it has also been reported that generic formulations in saline solution exhibit lower retention rates of PGE_1 in lipid particles and weaker pharmacological activity in animal models than innovator formulations (Takenaga et al., 2007). Therefore, it is important to investigate the difference in pharmaceutical quality between innovator and generic formulations.

In the Japanese Pharmacopoeia, the diameter of lipid particles in a lipid emulsion is defined as being below 7 μm. Included in the tests for the preparation of a parenteral lipid emulsion is "Insoluble Particulate Matter Test for Injections" as well as "Test for Extractable Volume of Parenteral Preparations". The former test defines an examination by "Method 1. Light Obscuration Particle Count Test" or

* Corresponding author. Tel.: +81 3 3700 8486; fax: +81 3 3707 6950.
E-mail address: h-shibata@nihs.go.jp (H. Shibata).

0378-5173/$ – see front matter © 2009 Elsevier B.V. All rights reserved.
doi:10.1016/j.ijpharm.2009.05.026

Table 1
Formulas of Lipo-PGE_1.

	Alprostadil (PGE1)	Purified soybean oil	Purified olive oil	Highly purified soybean lecithin	Oleic acid	Concentrated glycerin
Formulation #1 (innovator)	5 μg	100 mg		18 mg	2.4 mg	22.1 mg
Formulation #2 (innovator)	5 μg	100 mg		18 mg	2.4 mg	22.1 mg
Formulation #3 (generic)	5 μg		100 mg	18 mg	2.4 mg	22.1 mg
Formulation #4 (generic)	5 μg		100 mg	18 mg	2.4 mg	22.1 mg

"Method 2. Microscopic Particle Count Test". Method 1 is preferably applied to injections and parenteral infusions. However, in cases where the preparation has a reduced clarity or increased viscosity, such as emulsions, colloids and liposomal preparations, the test should be carried our according to Method 2. The Pharmacopoeia of the United State of America (USP), ⟨788⟩ also defines a similar method for parenteral preparations. However, within recent years, ⟨729⟩ "Globule Size Distribution in Lipid Injectable Emulsions" is listed in the second supplement of USP30. This ⟨729⟩ provides two methods, "Method 1. Light-Scattering Method" for the mean diameter of lipid particles, and "Method 2. Measurement of Large Globule Content by Light Obscuration or Extinction method" for the extent of large-diameter particles (>5 μm), and is required to meet both criteria. This is based on the idea that the size of the lipid particles is critical because large-size fat globules can become trapped in the smallest of blood vessels such as capillaries with diameters between 4 and 9 μm (Guyton, 1991). The essential size characteristics of a lipid injectable emulsion include the mean diameter of lipid particles and the range of the various particle diameters distributed around the mean diameter (Driscoll et al., 2001). In this study, we investigated the formation of aggregates and measured the mean diameter and/or number of large-diameter particles. We also monitored PGE_1 retention rate in Lipo-PGE_1 to investigate the difference in the pharmaceutical quality of Lipo-PGE_1 formulations.

2. Materials and methods

2.1. Materials

Four Lipo-PGE_1 formulations as shown in Table 1 were used in this study. Palux® injection (Formulation #1, lot nos. O17H2 and I07H2, Taisho Pharmaceutical Co., Ltd., Tokyo, Japan), Liple® injection (Formulation #2, lot nos. P625J and P205H, Mitsubishi Tanabe Pharma Corporation, Osaka, Japan), Alyprost® injection (Formulation #3, lot nos. AB07A and AF07A, Nippon Chemiphar Co., Ltd., Tokyo, Japan), Prink® injection (Formulation #4, lot nos. 659109 and 659123, Taiyo Yakuhin Co., Ltd., Nagoya, Japan) were purchased from a drug seller in Japan. Otsuka normal saline, Aminofluid®, Lactec® injection and Meylon® (Otsuka Pharmaceutical Co., Ltd., Tokyo, Japan), Amicaliq® (Termo Corporation, Tokyo, Japan), Solita®-T No. 3 (Ajinomoto Co., Inc., Tokyo, Japan), Hartmann's Solution pH 8 and Nipro infusion set IS type (Nipro Pharma Corporation, Osaka, Japan), were purchased from a general sales agency for drugs in Japan. Lactec® injection with $NaHCO_3$ was composed of 500 ml Lactec® injection and 20 ml Meylon® (7% $NaHCO_3$ injection). The official PGE_1 reference standard was purchased from the Society of Japan Pharmacopoeia. Slide-A-Lyzer® Dialysis Cassette (molecular weight cutoff: 7 K, capacity: 0.1–0.5 ml) and Buoy used for dialysis method were purchased from Pierce (IL, US). Disposable syringes, 21- and 27-gauge needles were purchased from Terumo Corporation.

2.2. Particle size distribution analysis

A 2 ml aliquot of Lipo-PGE_1 was injected into a 500 ml infusion bag of different solutions. After mixing, the various solutions were incubated at room temperature. At the indicated time point, each mixed solution was collected and analyzed by measurement of dynamic light scattering or single particle optical sizing.

2.2.1. Dynamic light scattering (DLS)

The particle size distribution and mean diameter of each Lipo-PGE_1 after mixing with different solutions were measured using a dynamic light scattering photometer DLS-7000 (Otsuka Electronics Co., Ltd., Osaka, Japan) equipped with a He–Ne laser source (wavelength, 632.8 nm). All DLS measurements were made with a scattering angle of 90°. Mixed solutions were diluted 15-fold with each infusion solution in order to obtain an appropriate scattering intensity. Data were gathered using a counting period of 100 s. Histogram analyses were performed to calculate the average particle size and standard deviation.

2.2.2. Single particle optical sizing (SPOS)

An Accusizer 780A (Particle Sizing Systems, Santa Barbara, CA) was used to determine the number of large-diameter particles in the emulsions. This instrument is based on light extinction (LE) or light scattering (LS) that employs a single-particle optical sizing (SPOS) technique, and was equipped with an automatic dilution system. In this study, the summation mode, which is a combination of LE and LS, was applied to measure the number of particles >0.5 μm in diameter. Before commencing any measurements, the equipment was filled with each infusion solution by using the command "Start Vessel Flush". After ensuring the background count was below 100 counts/s, mixed solutions (about 5 ml) were injected into the sample chamber. Duplicate measurements were made for each sample at the appropriate time point using the following conditions; data collecting time, 60 s; flow rate, 60 ml/min; injection loop volume, 1.04 ml; syringe volume, 2.5 ml; second dilution factor, 40. We ascertained that this dilution factor maintained the per-milliliter counts below the coincidence limit for the sensor, thereby minimizing this source of error. The volume-weighted proportion of fat globules (PFAT) with a diameter of >5 μm ($PFAT_5$) was calculated by the command "Volume Fraction cal".

2.3. Zeta potential

Zeta potential was measured using a Zetasizer NanoZS (Malvern Instruments, Malvern, UK), which is based on laser Doppler velocimetry in an electric field. For each Lipo-PGE_1, 500 μl was diluted using 10 ml distilled water.

2.4. Determination of PGE_1 retention rate

2.4.1. Assay for PGE_1

PGE_1 was measured by high-performance liquid chromatography (HPLC) using a post-column reaction. The HPLC system consisted of two constant pumps (LC-10ADvp, Shimadzu, Kyoto, Japan), a degasser (DGU-14A, Shimadzu), an automated pretreatment system, an autoinjector (SIL-10ADvp, Shimadzu), a UV/VIS detector (SPD-20AD, Shimadzu), a column oven (CTO-10ACvp, Shimadzu), and a system controller (SCL-10Asp, Shimadzu). PGE_1 was detected at 278 nm. The column used in this study was a 15 cm stainless-steel (4.6 mm i.d.) 5 μm Ø Mightysil ODS (Kanto Chem-

Table 2
Compositions of infusion solution.

	g/500 ml												
	NaCl	KCl	$CaCl_2$	$MgCl_2$	$C_3H_5NaO_3$	$C_{12}H_{22}CaO_{14}$	K_2HPO_4	$MgSO_4$	ZnSO4	Amino acids	Glucose	pH	mequiv./L
Normal saline	4.50	–	–	–	–	–	–	–	–	–	–	6.0	1
AMINOFLUID®	0.39	–	–	–	1.15	0.41	0.56	0.31	0.70	15.00	37.50	6.7	3
AMICALIQ®	–	0.82	–	0.15	1.41	0.13	–	–	–	13.75	37.50	4.6–5.6	3
SOLITA®-T No. 3	0.45	0.75	–	–	1.12	–	–	–	–	–	21.5 0	3.5–6.5	1
Hartmann's solution pH 8	3.00	0.15	0.10	–	1.55	–	–	–	–	–		7.8–8.2	1
Lactec® Injection	3.00	0.15	0.10	–	1.55	–	–	–	–	–		6.0–8.5	0.9
MEYLON®	$NaHCO_3$	1.4 g/20 ml										7.0–8.5	5

ical Co., Inc., Tokyo, Japan) with a 10 m Teflon tube (0.5 mm i.d.) as a post-column. The automated pretreatment system consisted of a pretreatment column, a constant pump for cleaning solutions, and two switching valves. The pretreatment column used was a 2.5 cm stainless-steel (4.0 mm i.d.) 5 μm Ø LiChroCART 25-4 Lichrospher 100RP-18e (Merck, Darmstadt, Germany). The mobile phase consisted of acetonitrile:1/150 M phosphate-buffered solution (pH 6.3). The ratio of organic to aqueous phase was 28:72 (v/v). 1 M KOH was used for the reaction solution. Special grade ethanol (99.5%) was used for the cleaning solution. The flow rate of the mobile phase, reaction solution, and cleaning solution were 1.0 ml/min, 0.5 ml/min and 2.0 ml/min, respectively. The temperature of both columns was approximately 60 °C. A 50 μl aliquot of a two-fold diluted sample in mobile phase was injected. This system was constructed in accordance with the first supplement of the Japanese Pharmacopoeia (15th edition).

2.4.2. Dialysis method

Rate of PGE_1 retention in lipid particles was measured by a dialysis method. 340 μl of Lipo-PGE_1 was injected into a dialysis cassette, immersed in 85 ml of each infusion solution, and incubated with gentle agitation at 20 °C in a water bath. Each dialysis cassette was floated by using a buoy. After incubation for the indicated time the dialysis cassette was retrieved and the concentration of PGE_1 inside the cassette measured using the HPLC method described earlier. A 5 μg/ml solution of PGE_1 in normal saline was also injected into a dialysis cassette, incubated for the indicated time, and then the concentration of PGE_1 in the cassette measured as Lipo-PGE_1. The rate of PGE_1 retention was calculated in comparison with the 0 time sample, after correction for changes in volume of solution in the dialysis cassette.

3. Results and discussion

Firstly, we investigated whether the intravenous line becomes clogged by a suspention of generic Lipo-PGE_1 formulations and Hartmann's solution pH 8. A 2 ml solution of Formulation #1 (innovator) or Formulation #3 (generic) was injected into a 500 ml infusion bag of "Hartmann's solution pH 8." After mixing, an infusion set was attached to each infusion bag and the roller clamp was fully opened. In the suspension of Formulation #1, no decrease in drip rate or accumulation of aggregated substances in the infusion line was observed. By contrast, the drip rate of a suspension of Formulation #3 significantly decreased after 1 h and had completely stopped after 2 h. Additionally, a white aggregation substance was observed in the infusion line of the suspension of Formulation #3 (Fig. 1). Thus, we confirmed the previously reported phenomena.

We reasoned that an increase in the diameter of lipid particles in the infusion solution was likely to cause a decrease in the drop rate and the formation of aggregates. Therefore, after mixing of Lipo-PGE_1 with infusion solution, the time-dependent change in the mean diameter of lipid particles in the suspension was measured by dynamic light scattering (DLS) (Fig. 2). Seven different infusion solutions were used in this study as listed in Table 2. Hartmann's solution pH 8 and Ringer's lactate with sodium bicarbonate solution were included, which have been reported to cause aggregates and blockages in the infusion line. The mixing of Lipo-PGE_1 with Aminofluid® or Amicaliq® induced no obvious alteration in the size of the lipid particles over time, although the mean diameter was slightly greater compared to that observed using normal saline. The slightly greater diameter of the Lipo-PGE_1 particles in the presence of Aminofluid® or Amicaliq® is presumably caused by an accumulation of positively charged substances, such as arginine, histidine, Mg^{2+} and Zn^{2+}, around the lipid particle. In the case of Solita-T® No. 3 and Lactec® Injection, the mean diameter of the lipid particles was unchanged compared with that observed in normal saline. The mixing of Formulation #3 or Formulation #4 with the mixture of Lactec® injection and Meylon® (a 7% sodium bicarbonate injection) transiently increased the mean diameter of the lipid particles, although that of innovator formulations did not. Interestingly, there was no significant increase in the mean diameter of lipid particles in Hartmann's solution pH 8.

Next, the number of large diameter lipid particles was determined in suspensions of Lipo-PGE_1 in infusion solution using a single-particle optical sensing (SPOS) method. The number of lipid

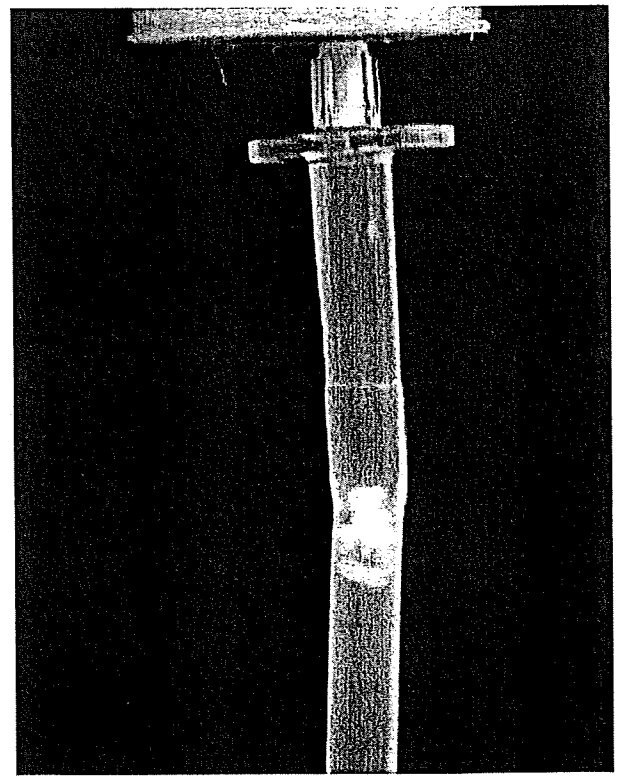

Fig. 1. Photograph of aggregation substances in suspension with Formulation #3 and Hartmann's solution pH 8.

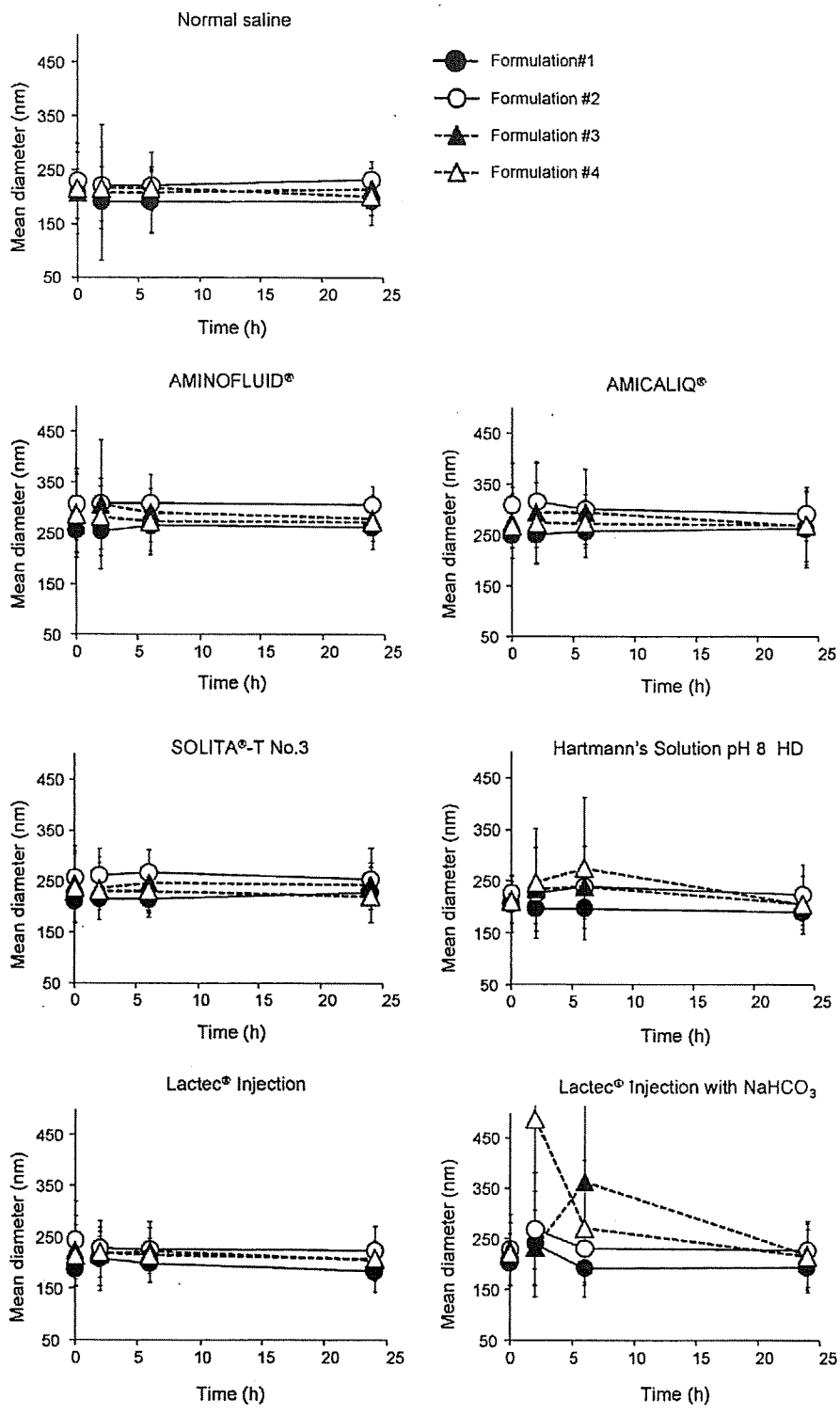

Fig. 2. Mean diameter of Lipo-PGE_1 after mixing with each infusion solution. Lipo-PGE_1 was mixed with each infusion solution and incubated at room temperature. Data represent the mean ± SD.

particles with a diameter >0.5 μm or >1 μm in an emulsion of Lipo-PGE_1 with each infusion solution is shown in Figs. 3 and 4, respectively. Intriguingly, the particle number >0.5 μm of generic formulations was larger than that of innovator formulations in all of the infusion solutions tested, while the particle number >1 μm of generic formulations was clearly smaller than that of innovator formulations in most of the infusion solutions, except Hartmann's solution pH 8 and Lactec® injection with Meylon®. Mixing generic formulations in Hartmann's solution pH 8 HD caused a significant increase in particle number especially with a diameter >1.0 μm. However, the particle number >1.0 μm of innovator formulations remained unchanged, although the particle number >0.5 μm of For-

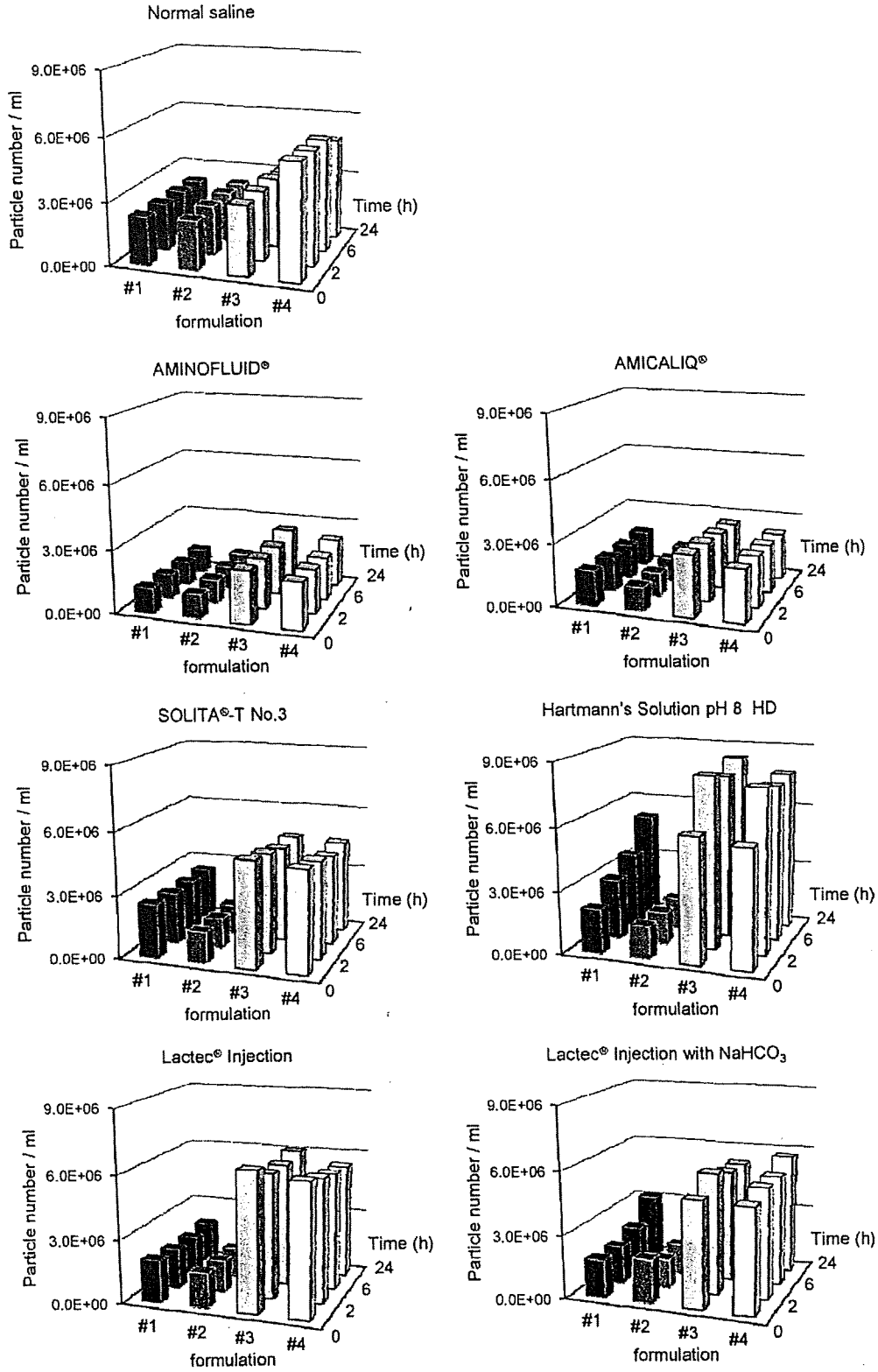

Fig. 3. Effect of each infusion solution on the total particle number of Lipo-PGE_1. The counts per milliliter per size range were normalized to the undiluted sample. Data represent the mean of two samples. Error bars were omitted by reason of the small standard deviations.

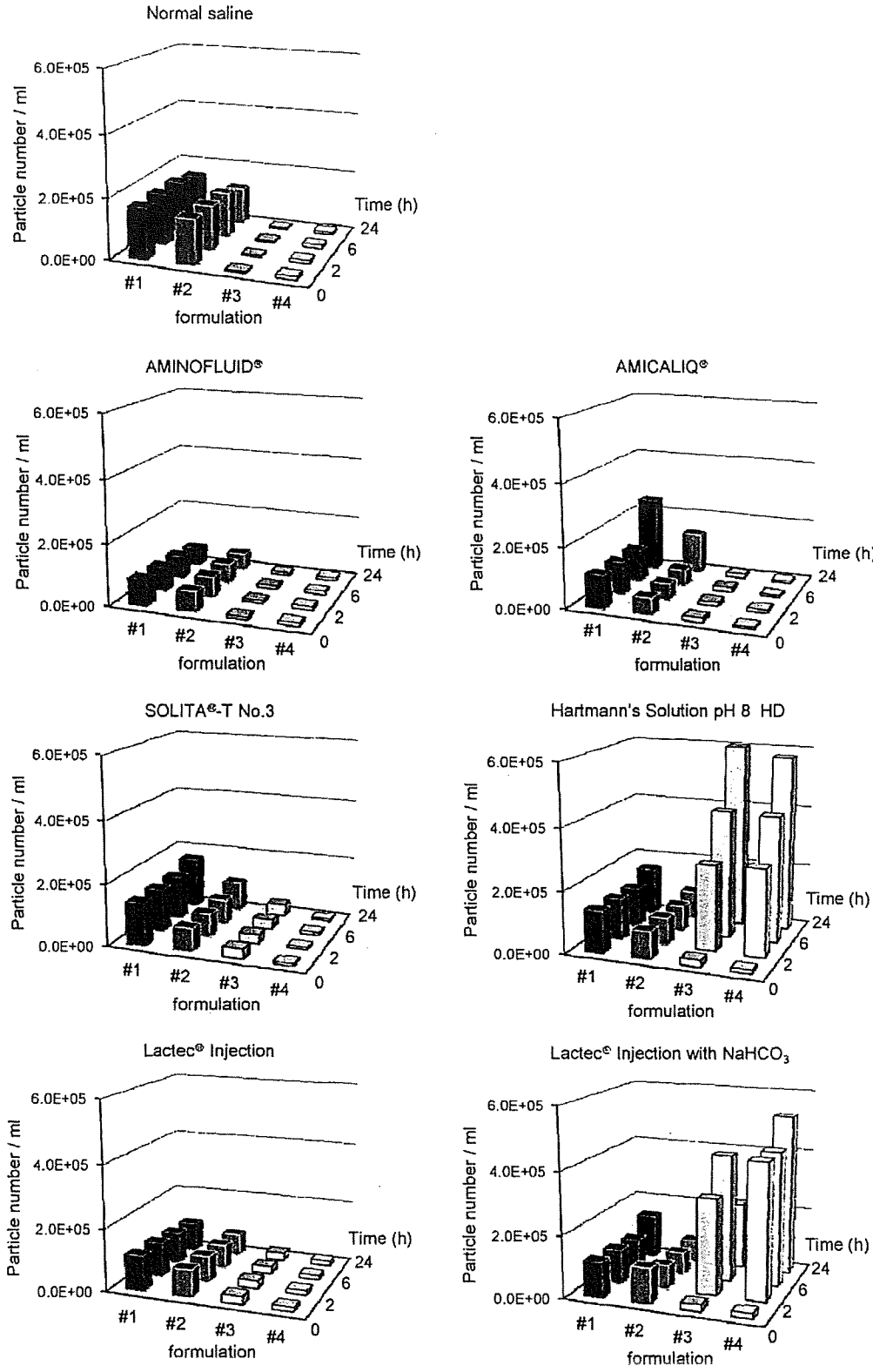

Fig. 4. Effect of each infusion solution on the large particle (diameter > 1.0 μm) number of Lipo-PGE_1.

mulation #1 gradually increased over time. Furthermore, in Lactec® injection with Meylon®, the particle number >1.0 μm of generic formulations increased markedly. Fig. 5 shows the particle distribution in an emulsion of each formulation with Hartmann's solution pH 8 or Lactec® injection with Meylon®. Among the innovator formulations, the distribution curve of Formulation #2 was unchanged, even 24 h after mixing, although that of Formulation #1 displayed an increase in the number of large particles. For the generic for-

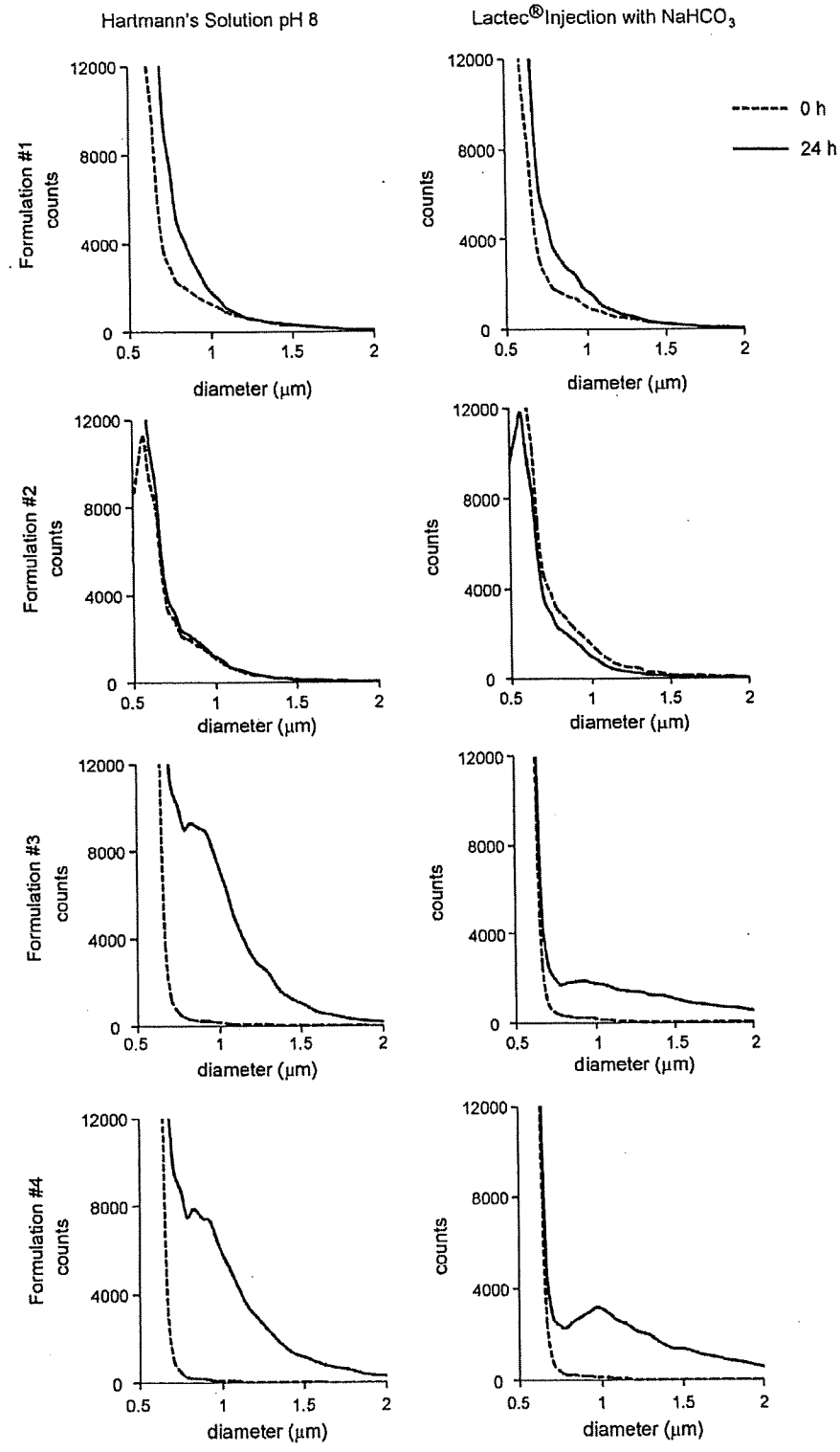

Fig. 5. distribution of Lipo-PGE_1 in Hartmann's solution pH 8 or Lactec® Injection with $NaHCO_3$. Dashed lines show 0 time, and full lines show 24 h after mixing with Lipo-PGE_1 and each infusion solution.

mulations, a significant increase of lipid particles of around 1 μm in diameter or a broad distribution of large particles was observed in Hartmann's solution pH 8 or Lactec® injection with Meylon®, respectively. These results indicate that the increase in the size of the lipid particles is related to the infusion solution used. The change in the size of the lipid particles in Amicaliq® was observed over a period of time. The particle number of innovator formulations increased 24 h after mixing, while that of generic formulations did not. In other infusion solutions there were no change in the particle number.

Table 3
Volume-weighted percentages of lipid particles with a diameter of >5 μm ($PFAT_5$) 2 h after suspension.

Lipo-PGE_1	Normal saline	Mean ± S.D.	
		Hartomann's solution pH 8 HD	Lactec® Injection with $NaHCO_3$
Formulation #1	0.025 ± 0.006	0.026 ± 0.002	0.009 ± 0.001
Formulation #2	0.006 ± 0.001	0.007 ± 0.001	0.007 ± 0.001
Formulation #3	0.034 ± 0.002	0.014 ± 0.004	0.056 ± 0.004
Formulation #4	0.012 ± 0.003	0.008 ± 0.001	0.012 ± 0.002

These results indicate that the substantial increase in the number of large particles is a potential factor leading to the aggregation of substances in the infusion line and slowing of the drip rate. Moreover, our studies revealed that, even using innovator formulations, the mixing of Formulation #1 with Hartmann's solution pH 8 increased the number of large particles at some level. Thus, in some cases, the SPOS method could detect changes in the number of large particles that could not be detected by the measurement of mean diameter or size distribution using DLS. Our data also indicate that the SPOS method may be a useful means of assessing the formulation stability of emulsions or the incompatibility with infusion solutions. Although the actual number of particles is given in this study, in USP ⟨729⟩, the instrument range of detection is set at 1.8–50 μm, and the volume-weighted percentage of lipid particles greater than 5 μm ($PFAT_5$) must be less than 0.05%. Thus, the $PFAT_5$ of each Lipo-PGE_1 formulation was calculated after mixing with normal saline, Hartmann's solution pH 8, or Lactec® injection with Meylon® (Table 3). Only the $PFAT_5$ of Formulation #3 in Lactec® injection with Meylon® was more than 0.05%, and the $PFAT_5$ of even generic formulations did not exceed 0.05%. This is because there was a significant increase in the number of lipid particles around 1 μm in diameter in the emulsion of generic formulations with Hartmann's solution pH 8. Such emulsion conditions could result in a blocked infusion line or at least some build-up of aggregation substances. Therefore, a measurement of the number of particles not only larger than 5 μm but also around 1 μm will be required depending on the particular situation. Large particles ranging from dozens to several hundred μm in diameter, which can clog the infusion line directly, were not detected in our study. There is a possibility that the partial accumulation of lipid particles around 1 μm may trigger a blockage in the infusion line. However, we could not eliminate the existence of large particles that are not detected by the SPOS method because they may be unstable in the very high flow rates used in this technique. Nevertheless, the assessment of emulsions using the SPOS method will simplify the procedure and allow the detection of a wide distribution of particle sizes.

One factor that may increase the number of large particles in the emulsion of generic Lipo-PGE_1 but not innovator Lipo-PGE_1 under alkaline conditions in the presence of calcium ions, such as Hartmann's solution pH 8 or Lactec® injection with Meylon®, is the zeta potential of the particle surfaces. As is well known, an electric charge on the particle surface brings about inter-particle repulsion, thereby preventing aggregation (Washington et al., 1989; Washington, 1990). If the electric charge of the particles in the emulsion is small, the stability of the emulsion will decrease. Thus, the zeta potential of each Lipo-PGE_1 formulation in water was measured (Table 4). Surprisingly, there were no significant differences between innovator and generic formulations. Indeed, the zeta potential of the generic formulations was slightly lower than that of the innovator formulations. This result indicates at least that the difference of zeta potential in normal saline may not be a factor causing the difference in stability between generic and innovator formulations under alkaline conditions in the presence of calcium ions. To clarify the effect of zeta potential on the formation of aggregation, the zeta potential value of each formulation in all infusion solutions as well as various pH solutions in the presence or absence of calcium ions should be measured as a subject of future investigation. Other factors include not only the difference in the method for manufacturing or the control of the process, but also a difference in the formulation. While the lipid particle of innovator formulations is composed of soybean oil, that of generic formulations is composed of olive oil as shown in Table 1. These two kinds of plant oil seem to have some differences in their physical characteristics because the main fatty acid of soybean or olive oil is linoleic acid or oleic acid, respectively. All additives in the generic formulations, except the oil, are exactly the same as innovator formulations. The hydrophile–lipophile balance (HLB) of emulsifier or oil as well as temperature and pH is important for the stability of the emulsion (Griffin, 1954; Becher, 1957). Thus, there is a possibility that the change of plant oil might bring about an alteration in the appropriate HLB of lecitin, and cause instability within the emulsion such as aggregation. Additionally, the HLB of lecitin is not constant like 7–13, because lecitin is a mixture of emulsifiers. Therefore, the HLB, relative proportion, or purity of lecitin might bring about the observed difference in stability. In either case, a detailed investigation will be required to reveal the cause of the increase in the number of large particles in generic formulations under alkaline conditions in the presence of calcium ions.

One report suggests that the PGE_1 retention rate of generic formulations in lipid emulsions is lower than that of the innovator formulations (Takenaga et al., 2007). Lipo-PGE_1 should be present at a high concentration within a lesion and maintain the concentration and activity of PGE_1 in the circulatory system. Stable retention of PGE_1 within the lipid particle is very important for exhibiting clinical effectiveness. Thus, the PGE_1 retention rate was measured in normal saline, Solita®-T No. 3, and the infusion solution in which the number of large particles increased, such as Amicaliq®, Hartmann's solution pH 8, and Lactec® injection with Meylon® (Fig. 6). The PGE_1 retention rates were measured using either the filtration, dialysis, or ultrafiltration method in previous reports (Takenaga et al., 2007; Igarashi et al., 1988; Yamaguchi et al., 1995; Teagarden et al., 1988). In the filtration method, the sample is passed through a membrane filter with a pore size of 0.1 μm connected to a disposable syringe. However, smaller particles may pass through the filter unit causing the data to fluctuate depending on the precise force applied to the syringe. In this study, the PGE_1 retention rate was measured by the dialysis method. Compared to a solution of PGE_1, each formulation clearly retained PGE_1 in lipid particles in normal saline, Solita®-

Table 4
Zeta potential of Lipo-PGE_1.

Peak position	Formulation #1 (innovator)	Formulation # 2 (innovator)	Formulation # 3 (generic)	Formulation # 4 (generic)
Mean (mV)	−23.1	−24.5	−29.5	−28.3
Width (mV)	6.0	7.1	6.1	4.9

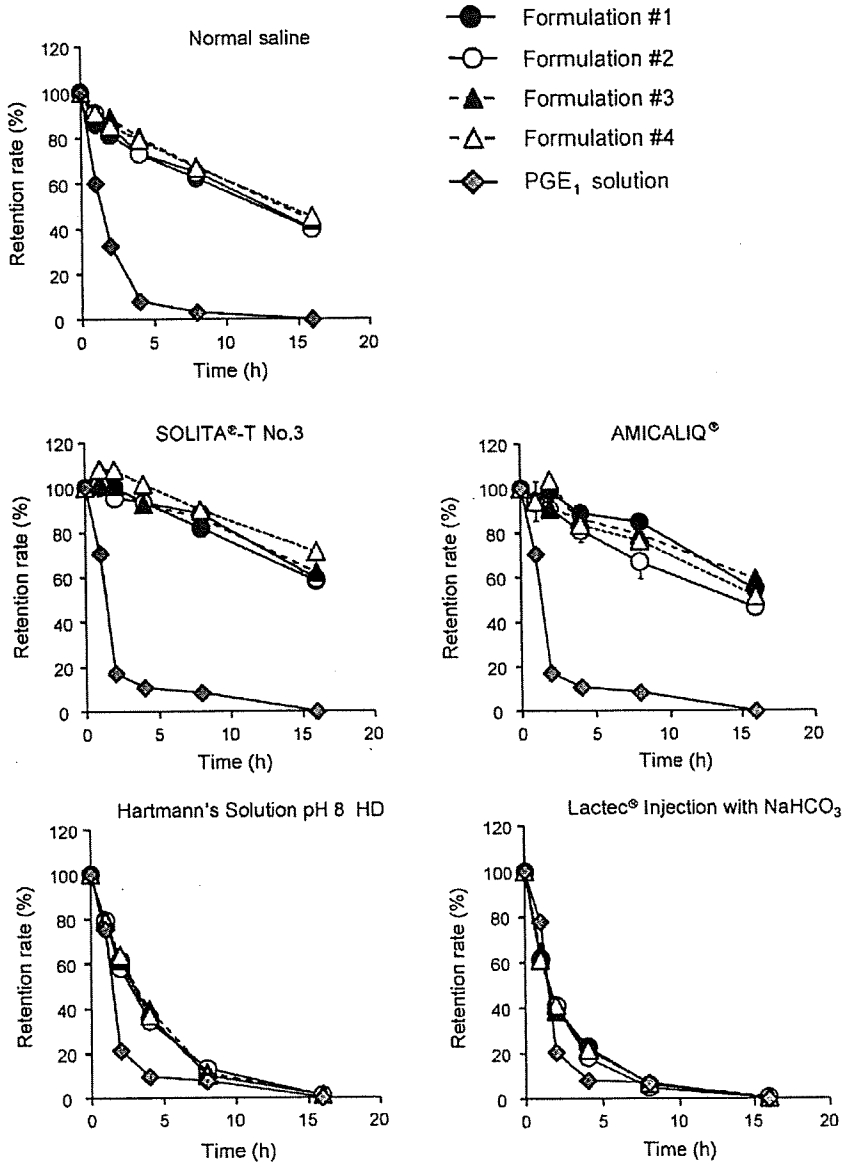

Fig. 6. Retention rate of PGE_1 in lipid particles in each infusion solution. Retention rate of PGE_1 in lipid particles of Lipo-PGE_1 was measured by the dialysis method at 20 °C. Plots show mean ± SD of percentages for three individual experiments. Solution PGE_1 (closed diamond) was used for a control of Lipo-PGE_1.

T No. 3 and Amicaliq® (Fig. 6). Moreover, there were no significant differences between formulations in these three infusion solutions. PGE_1 was rapidly released from lipid particles in Hartmann's solution pH 8, and Lactec® injection with Meylon®. Indeed, almost no PGE_1 remained in the lipid particles after 8 h. These results correlate with previous reports which indicated that the PGE_1 retention rate was influenced by the pH of buffered solution (Yamaguchi et al., 1995). This is because in alkaline condition PGE_1 ($pK_a = 4.89$) is anionic form and readily released from lipid particled while in acidic condition PGE1 is nutral form and mainly distributed to the oil/water interface (Teagarden et al., 1988). Even in these two infusion solutions, in which an increase in the number of large particles was observed, differences in the PGE_1 retention rate between innovator and generic formulations were not detected. Therefore, our results indicate that the PGE_1 retention rate of generic formulations is no lower than that of the innovator formulations.

Our study shows that the marked increase of large diameter (>1 μm) particles is a likely reason for the slowing of the drip rate and aggregation of substances in an infusion line of generic formulations under alkaline conditions in the presence of calcium ions. Moreover, our study indicates that a measurement of the number of large particles is very effective in assessing the stability of an emulsion. We also show that the mixing of Lipo-PGE_1 with Hartmann's solution pH 8 or Lactec® injection with Meylon® significantly decreased the retention rate of PGE_1 in lipid particles compared to normal saline. This decreased retention rate of PGE_1 is undesirable if Lipo-PGE_1 is to exert its full clinical effectiveness. Actually, the mixing of Lipo-PGE_1 with medicines other than infusion solution is restricted according to the package insert. However, the application of Hartmann's solution pH 8 is unrestricted because it is an infusion solution. Care must be taken over the choice of infusion solution due to the increase in the number of large particles generated using the generic formulations. Furthermore, it is preferable to administer Lipo-PGE_1 at as low a dilution as possible. In conclusion, except under alkaline conditions in the presence of calcium ions, there is no difference in mixing any infusion solu-